Experimental and Computational Investigation of Ultrasonic Welding of Short Carbon Fiber Reinforced Plastics

by

Tae Hwa Lee

A dissertation submitted in partial fulfillment
of the requirements for the degree of
Doctor of Philosophy
(Mechanical Engineering)
in the University of Michigan
2020

Doctoral Committee:

Research Associate Professor Mihaela Banu, Co-Chair
Professor S. Jack Hu, Co-Chair
Dr. Blair E. Carlson, General Motors
Professor Albert J. Shih
Professor Alan I. Taub

Tae Hwa Lee

taehwale@umich.edu

ORCID iD: 0000-0003-2280-6374

Acknowledgements

Above all, I would like to express my sincere thanks to my advisors, Professor S. Jack Hu and Professor Mihaela Banu. Since I started my Ph.D. program, Professor S. Jack Hu has provided me a lot of opportunities to grow as a good researcher and engineer. He is a great teacher and scientist who always motivates me to develop my abilities to handle the difficulties that I faced while conducting my research. Also, his gentleness and patience to take care students made it easy to communicate with him, as such I was able to have a lot of valuable discussions despite of his busy schedules as vice president for research in University of Michigan, and even after he moved to University of Georgia as senior vice president for academic affairs and provost.

I am also grateful to Professor Mihaela Banu. Even before the beginning of my study as a Ph.D. student, she was really supportive and provided all the resources to conduct the research. She always considered her students as her first priority. Her kindness and willingness to help students led me to discuss with her for countless hours which helped me to resolve complex research problems. She provided me tremendous chances to improve my research skills and knowledge. None of my Ph.D. works would have been achieved without her help.

I also appreciate to my committee members, Professors Albert Shih, Professor Alan I. Taub and Dr. Blair E. Carlson for spending their time to evaluate my dissertation and giving valuable advice. This study was sponsored by General Motors Collaborative Research Laboratory at the University of Michigan, Project No. N017367-ADVMAN-Automotive Collaborative Research Laboratory. I express additional thanks to General Motors for the financial support and the internship opportunities.

I also thank Dr. Pei-Chung Wang who was my advisor in General Motors during the internship. I would like to thank Dr. Hua-Tzu Fan, Dr. Guoxian Xiao and Dr. Jorge Arinez who supported me in General Motors for my research in the beginning of Ph.D. program.

I would like to acknowledge to all the Hu Lab members. The major progress of my research was built through the valuable discussions and interactions with the lab peers. I extend my gratitude to Jaekwang Shin who was a good friend and an excellent colleague. With his help and support, I could find solutions for my research. I also appreciate to Chanbai Tan who was supportive and didn't hesitate to discuss any topics. I would like to thank to Dr. Yang Li for close collaborations and discussions in several research papers. And I would like to share appreciation to Daniel Shriver who was a master student and transferred his research data to me with kind explanations in the beginning of my Ph.D. program. I also thank to Dr. Haseung Chung, Dr. Theodor Freiheit, Dr. Baicun Wang, Ying Luo, Lei Sun, Weiling Wen, and Lynn Cook for their kindness and willingness to help.

I would also like to thank the members of the Korean Presbyterian Church in Ann Arbor who were the supporting group for me and my family in any circumstances. I would like to acknowledge financial support from LG Hausys during my Ph.D. program. Especially, I would like to extend my gratitude to Dr. Heejune Kim who was my supervisor and always encouraged me.

More importantly, I should say my deepest thanks to my family for their faithful support and love. My parents and mother-in-law have been supporting me with their prayers. Finally, I would like to dedicate this dissertation to my wife, Yeo Jin Bae and my precious daughter, Daisy, who mean everything to me.

Table of Contents

List of Tables

List of Figures

Abstract

Carbon fiber reinforced plastics (CFRP) have been used in various industries due to its beneficial mechanical properties for light-weighting. Joining of CFRP is one of the most critical barriers for high volume application because the joining technologies used for metallic structures are not feasible for CFRP. Ultrasonic welding (USW) is a friction welding technology in that parts to be joined are clamped together under a trigger force and subjected to a high frequency vibration through the oscillation of a horn, leading to heating and melting of the material for bonding. USW is fast, clean, and suitable for automation, thus is attractive to the automotive industry for high volume production. Ultrasonic welding generally uses energy directors on the surfaces of the parts to be joined by concentrating the energy to help melting. Despite the positive role of energy directors on weld formation, their manufacture involves additional costs related to tools and equipment. Moreover, their presence at the interface between the specimens modifies the composite structure locally, leading to a non-uniform distribution of fibers in the weld area. Hence, the current industrial practice seeks to eliminate the use of energy directors. However there has been limited research of ultrasonic welding for CFRP without energy directors. Therefore, this dissertation focuses on understanding the mechanism of ultrasonic welding of CFRP without energy directors.

In this dissertation, three research topics are addressed:

(1) *Influence of morphological parameters on welding process and weld performance of CFRP by ultrasonic welding*: The research investigates the influence of degree of crystallinity and the crystalline phase weight ratio of CFRP (here, α/γ ratio for Nylon 6) on welding performance experimentally. An annealing process is used to control the degree of crystallinity and the crystalline phase weight ratio with various annealing temperatures

and heating speeds. With the changes of morphological parameters, the mechanical properties and viscoelastic properties are measured to investigate the influence of morphological parameters on the ultrasonic welding process and its performance.

(2) *Process modeling of ultrasonic welding of carbon fiber reinforced plastics without energy directors*: A finite element method (FEM) model is created to investigate the heating phenomena of ultrasonic welding process of CFRP without an energy director. The mechanical properties of CFRP are measured to create the FEM model in ABAQUS. The model is validated with experimental results of temperature and weld area evolution in ultrasonic welding of CFRP. Different morphological parameters will be used in FEM model to investigate the impact of morphological parameters in ultrasonic welding of CFRP.

(3) *Dynamic analysis of ultrasonic welding of CFRP according to boundary conditions:* A dynamic FEM model is created to investigate the influence of natural frequency in ultrasonic welding of CFRP by varying the weld locations. The dynamic FEM model is used to calculate the natural frequencies near the vibration frequency with respect to the entire ultrasonic welding process. The dynamic FEM model results will be compared with the process FEM model results of ultrasonic welding in terms of heat generation depending on the effect of natural frequency.

This dissertation provides new understanding and insights to improve the process stability and quality in ultrasonic welding of CFRP without energy directors.

Chapter 1 Introduction

This dissertation investigates ultrasonic welding (USW) of carbon fiber reinforced plastics (CFRP) using experimental and computational methods. This chapter presents the motivation, summary of literature review, proposed research and approach, and expected contributions.

1.1. Motivation

Carbon fiber reinforced plastics, also called carbon fiber composites, have been used for lightweight purposes in the aerospace, automotive, and sporting goods industries due to the good mechanical properties such as specific modulus and strength compared with metallic materials [1-3]. The excellent mechanical properties of CFRP have enabled improvement in fuel efficiency and structural performance. But several challenges, such as a high raw material cost, lack of established high volume manufacturing and joining methods, and lack of proper composite design methods, need to be addressed in order for CFRP to be broadly used in industries [4].

Joining of CFRP is one of the most critical barriers because the joining technologies used for metallic structures are not feasible for CFRP [5]. There are three main joining technologies for CFRP which are mechanical joining, adhesive bonding, and fusion bonding [6]. Mechanical joining uses separate metallic or plastic fasteners and holes. The holes in CFRP causes stress concentration and drilling generates localized damage which leads to an initiation of fracture in CFRP. Inserted metallic fasteners in CFRP cause residual stress due to different coefficients of thermal expansion between CFRP and metallic materials. The metallic fasteners may be corroded

with CFRP more easily. In addition, metallic fasteners increase weights of assembled components which defeats the most important purpose of using CFRP for a weight reduction.

The adhesive bonding technology is a common method for joining CFRP. But the performance of adhesive joints depends on service temperature, moisture absorption, adhesive type, and curing cycle parameters [7]. The most common adhesives are thermoset types which are not feasible for recycling requirements and necessary to have a long curing time and difficulty in maintaining the required gap over an entire bond line in complex geometries.

Fusion bonding technologies can be a good candidate for CFRP based on thermoplastic matrix. Fusion bonding technologies use several different ways for heat generation. According to the energy sources of heating, fusion bonding technologies can be divided into three categories which are thermal welding, friction welding, and electromagnetic welding. Ultrasonic welding is one of friction welding technologies in that parts to be joined are clamped together under a trigger force and subjected to a high frequency vibration through the oscillation of the horn, leading to melting of the material for bonding [8].

Ultrasonic welding is fast, clean, and suitable for automation, thus is attractive to the automotive industry for high volume production. Ultrasonic welding generally uses energy directors on the surfaces of the parts to be joined to help melting by concentrating the energy. Despite the positive role of energy directors on weld formation, their manufacture involves additional costs related to tools and equipment. Moreover, their presence at the interface between the composites modifies the composite structure locally during welding, leading to a non-uniform distribution of fibers in the weld area [9, 10]. Hence, eliminating the use of energy directors will lead to process simplicity and lower cost.

Many researchers have studied the mechanism for heating and healing of materials in ultrasonic welding of CFRP. They also have focused their work on optimizations of process parameters to improve the weld quality of joining CFRP. Recently, some research was conducted for ultrasonic welding of CFRP in characterization of weld attributes and performance prediction of spot welds without energy directors [10, 11]. However there has been limited research of ultrasonic welding for CFRP without energy directors. Therefore, this dissertation focuses on understanding the mechanism of ultrasonic welding for CFRP without energy directors.

1.2. Summary of Literature Review and State of the Art

A detailed literature review will be presented in Chapter 2. A summary of main findings from the review is provided here.

Currently CFRPs are made with various reinforcements and polymeric matrix materials. The performance of CFRP depends mainly on the reinforcement types and the continuous fibers are preferred as they create advantages in performance. However, continuous fiber composites involve slower manufacturing processes. As such discontinuous fibers are more desired for mass production.

The mechanism of heating for ultrasonic welding of CFRP has been investigated by many researchers and the suggested theories are interfacial friction and intermolecular friction. However, the heating mechanism is relying on the workpiece materials and is still being debated.

The process parameters of ultrasonic welding are trigger force, welding energy (time), holding time, amplitude (or amplitude percentage) of horn oscillation, and welding speed. These parameters need to be controlled accurately and it is important to choose a proper combination of parameters.

Energy directors have been used to help welding by providing a locally compliant area compared to the workpieces. There are several types of energy directors depending on shape and size. There is limited research on ultrasonic welding of CFRP without energy directors even though many industries desire welding processes without the energy directors. USW process simulation models need to be developed to study the heating mechanism of CFRP without energy directors.

Models have been developed to study the heating phenomena of ultrasonic welding processes. Prediction models of performance based on weld attributes have been developed to reveal the relationship between weld attributes and weld strength.

The main mechanical impact of ultrasonic welding is the oscillation of horn. Dynamic analysis of the whole system including the workpieces, the horn and the fixture needs to be conducted due to the natural frequency of vibration. There have been several studies for the dynamic analysis of ultrasonic welding processes for metallic materials but not for polymeric materials.

1.3. Proposed Research

The main process parameters of ultrasonic welding include welding speed, trigger force, welding energy (time), hold time, and amplitude of vibration. Ultrasonic welding performance without energy directors depends on the process parameters and the properties of CFRP. CFRP are based on polymeric material matrix and their properties can be changed depending on the crystalline structures which are determined from prior processing even though the constituents and their ratio remain are the same. These parameters can be called morphological parameters such as degree of crystallinity and crystalline components ratio for semi-crystalline polymers.

An overview of proposed hypotheses of this research is shown in Figure 1.1. One of the hypotheses is that the welding performance is influenced by the process parameters and the

morphological parameters which influence the heating phenomena in ultrasonic welding of CFRP without energy directors. Beyond the scale of specimen dimension, the larger dimension of ultrasonic welding system needs to be investigated. The second hypothesis is that the welding performance is different depending on the locations and the welding sequence of ultrasonic welding in the welding system due to the different boundary conditions. Investigation of welding performance is carried out based on modal analysis to identify the natural frequency of the welding system which impacts significantly on the oscillation of horn and workpieces.

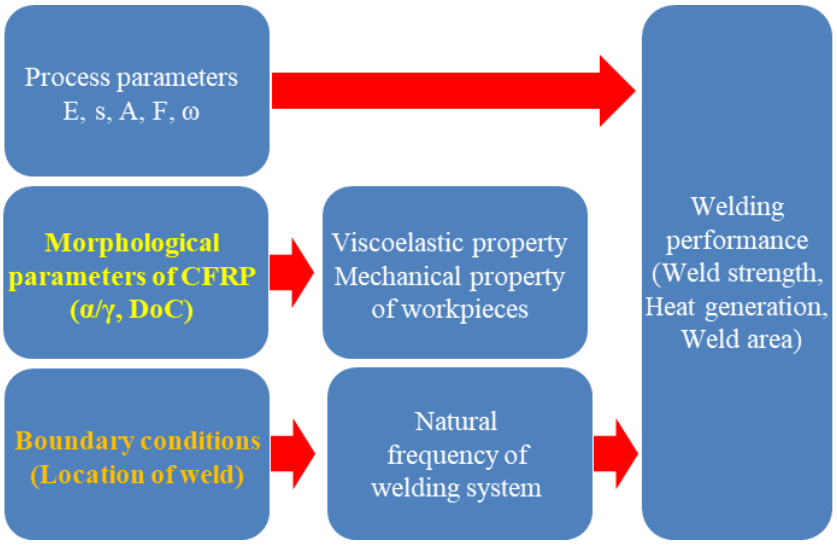

Figure 1.1 Overview of proposed hypotheses for this study (E: Welding Energy (J), s: Welding speed (mm/s), A: Amplitude (mm), F: Trigger force (N), ω: Frequency (Hz), α/γ: Weight fraction ratio of crystal α and γ, DoC: Degree of Crystallinity (%))

To investigate and validate the hypotheses, two research questions are to be addressed: (1) the importance of the morphological parameters in explaining the unstable and low welding performance of ultrasonic welding for CFRP without energy directors, and (2) the best means to investigate the influence of the parameters in the ultrasonic welding process of CFRP without energy directors.

1.4. Proposed Approach

To address two research questions, three research tasks are proposed as below:

(1) *Task 1*: Investigation of morphological parameters to understand the mechanisms for the unstable welding performance of CFRP by ultrasonic welding without energy directors;

(2) *Task 2*: Development of a FEM model to investigate the heating phenomena in ultrasonic welding of CFRP without energy directors;

(3) *Task 3*: Development of a modal analysis simulation model based on FEM model to investigate the natural frequency of ultrasonic welding of CFRP according to boundary conditions.

An overview of the proposed approach is presented in Figure 1.2, which shows the main research steps for the proposed tasks and the relationships of these tasks.

For ***Task 1***, degree of crystallinity and the crystalline phase weight ratio of CFRP (here, α/γ ratio for Nylon 6) are measured and investigated to understand their influence on welding performance experimentally. Annealing process is used to control the degree of crystallinity and the crystalline phase weight ratio with various annealing temperatures using a specific heating speed. With the changes of morphological parameters, the mechanical properties and viscoelastic properties are measured to investigate the influence of morphological parameters on the ultrasonic welding process and its performance.

In ***Task 2***, Finite Element Method (FEM) model is created to investigate the heating phenomena of ultrasonic welding process of CFRP without energy directors. The mechanical properties of CFRP are measured to create FEM model in ABAQUS. The model is validated with experimental results of temperature and weld area evolution in ultrasonic welding of CFRP.

Different morphological parameters will be used in FEM model to investigate the impact of morphological parameters in ultrasonic welding of CFRP.

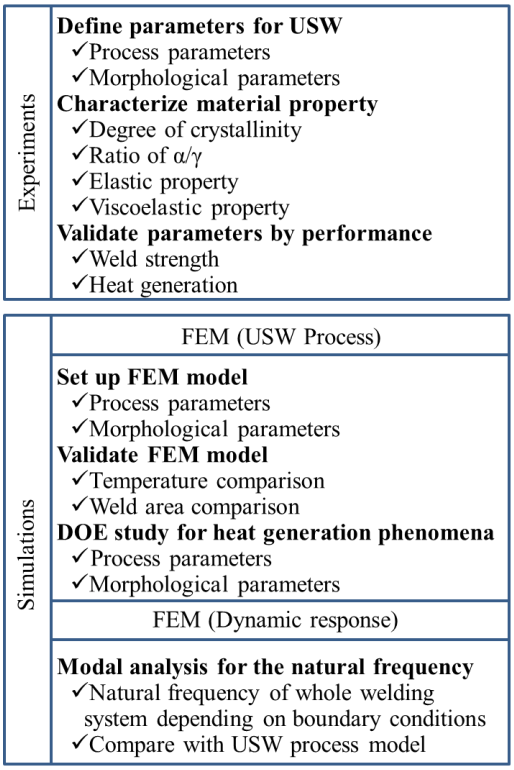

Figure 1.2 Overview of proposed approach

In ***Task 3***, FEM model is created to investigate the influence of natural frequency in ultrasonic welding of CFRP depending on the locations of welding. FEM model in ABAQUS is used to calculate the natural frequencies and their response near the vibration frequency in whole ultrasonic welding process. The results will be compared with the simulation results of ultrasonic welding process model in terms of heat generation depending on the effect of natural frequency.

1.5. Expected Contributions

The outcome of this research will be not only fundamental intellectual contributions but also practical contributions to the industries seeking suitable technologies for joining CFRP in high volume production. Since the ultrasonic welding of CFRP without energy directors has not been well investigated, the specific contributions of this study are expected as follows:

(1) understanding the heating phenomena in ultrasonic welding without energy directors;

(2) controlling and improving ultrasonic welding performance of CFRP without energy directors through introducing new parameters;

(3) modeling ultrasonic welding process according to morphological parameters;

(4) revealing the dynamic response of ultrasonic welding process in a large scale depending on the welding locations in consideration of the mass production.

1.6. Organization of Proposal

The rest of this proposal is organized as following. Chapter 2 will provide a detailed review of published literature as a basis for the state of the art in CFRP, theoretical background of ultrasonic welding for CFRP, and the modeling of ultrasonic welding. Chapter 3 will present investigation of new parameters to understand reasons for the unstable ultrasonic welding performance of CFRP without energy directors. Chapter 4 will develop a FEM model to investigate the heating phenomena in ultrasonic welding without energy directors. Chapter 5 will present a FEM model to study the dynamic modal analysis of ultrasonic welding of CFRP without energy directors. Chapter 6 will summarize the preliminary work and present the future work.

Chapter 2 Literature Review

This chapter provides a detailed literature review in areas relevant to the proposed research, including carbon fiber reinforced plastics (CFRP) and their joining technologies, theoretical background of ultrasonic welding of CFRP, and the modeling of ultrasonic welding of CFRP.

2.1. Carbon Fiber Reinforced Plastics and Their Joining Technologies

CFRP have been used for several decades in various industries and many researchers have studied the fabrication and the improvement of CFRP properties [12-14]. Composite materials typically consist of reinforcement and matrix. Glass fiber, carbon fiber, natural fiber, ceramic fiber, metal fiber and organic fiber are general choices for reinforcements based on polymer matrix. Among them, carbon fibers have the highest specific mechanical properties which lead to their uses in aerospace industry since 1970s. Polymers can be divided into two categories which are thermoplastic and thermoset polymers. The difference of the two is whether the polymers are re-melted after solidification or not. Thermoplastic can be re-melted but thermoset polymer cannot be re-melted after the crosslinking is completed. This section will provide a brief introduction of CFRP with thermoplastic matrix.

2.1.1. Reinforcement

Reinforcements in composite materials provide high mechanical properties such as stiffness and strength to maintain the structure against loading [15]. The shape of reinforcements is generally in fiber form and the fibers are grouped into a bundle of several thousand filaments for

convenient use. The length and diameter of fibers are dependent on their manufacturing process and component ratio. There are various fibers for composite materials but this research is only focused on carbon fibers.

Major properties of composite materials such as modulus and strength are dominantly dependent on the reinforcements. The volume fraction, direction, and length of reinforcements are key parameters for tailoring the mechanical properties of CFRP and determining the manufacturing process of CFRP applications. The shape of carbon fibers can be divided into 2 types which are continuous fiber and discontinuous fiber and the discontinuous fiber can be divided into long fiber and short fiber according to their length.

Continuous fibers are supplied in a shape of roving and used in the forms of woven fabric, non-crimp fabric, and tape with bonding materials to maintain their shape. Discontinuous fibers are generally supplied in forms of pellets or strand mixed with matrix materials to maintain uniform distribution of fibers in composite materials. Generally the length of short fibers is less than 1 mm and the long fibers have their length between 5mm and 25mm [16]. The shape of long fibers is used in direct compounding process where intermediate products like pellets are not used in order to reduce several manufacturing steps. Mat type reinforcement with long fiber is also used in sheet form and it provides higher modulus due to longer fiber length which is between 25mm and 100mm.

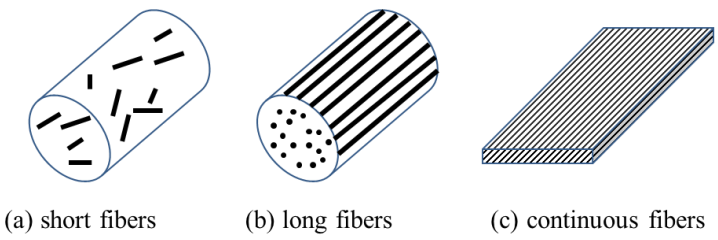

Figure 2.1 Fiber type in CFRP: (a) Short fibers, (b) Long fibers, (c) Continuous fibers

The continuous fibers can provide the maximum modulus and strength to CFRP. But the design of product is limited to sheet like or profile shapes and the manufacturing cost is high compared with manufacturing cost with discontinuous fiber type CFRP application. The price of continuous carbon fibers is also high so its applications are limited to the aerospace industries, limited volume luxury vehicles and sporting goods. Long fibers and short fibers provide inferior mechanical properties in composite materials compared to continuous fibers but the production cost including raw material and manufacturing process is much cheaper [17, 18].

Table 2.1 Influence of fiber type in CFRP

Fiber type	Length	Performance	Material cost of fiber	Manufacturing cost of CFRP
Short fiber	≤ 1mm	Low	Low	Low
Long fiber	≤ 25mm	Intermediate	Intermediate	Low
Continuous fiber	-	High	High	High

2.1.2. Matrix

The roles of matrix in composite materials are to maintain the shape of workpieces, to provide rigidity, and to protect reinforcements from environmental and chemical damage. And matrix materials transfer structural loads to reinforcements and endure shear loads dominantly. Polymer composite materials can be categorized according to their matrix materials such as thermoset and thermoplastic [19]. In this section, only thermoplastic matrix based polymers will be presented.

Thermoplastic polymers have several advantages such as high toughness, shorter manufacturing time, no need to keep in a freezer, good solvent resistance and reprocessing possibilities so that the attempts to use thermoplastic polymers in composite materials have been

increasing in spite of better mechanical properties of thermoset polymers than thermoplastic polymers [20, 21]. But thermoplastic polymers have high viscosity even at the processing temperature comparing to thermoset polymers so it is important that the selection of process and its parameters to reduce the viscous effect in manufacturing steps [17].

Thermoplastic polymers can be divided into two kinds which are amorphous and semi-crystalline polymers. Amorphous polymers have randomly distributed molecular chains without any oriented molecular structures [22]. Amorphous polymers are generally transparent and softened with heating above glass transition temperature without exact melting temperature. Semi-crystalline polymers have amorphous phase and crystalline phase at the same time and their ratio is called degree of crystallinity which is an important property for semi-crystalline polymers. The amount of crystallinity in semi-crystalline polymers depends strongly on the processing conditions. In general, the higher degree of crystallinity tends to yield higher modulus, higher yield strength, higher tensile strength, and better resistance to solvents and chemical. However, the higher degree of crystallinity also leads to lower elongation to failure and lower resistance to crack propagation. For semi-crystalline polymers, the decline in modulus above glass transition temperature is not as huge as that for amorphous polymers. Semi-crystalline polymers reveal a crystalline melting temperature where the modulus reduces rapidly. At higher temperatures, both amorphous and semi-crystalline polymers begin to degrade irreversibly and eventually decompose [16].

Amorphous polymers are not used well for composite materials because of low heat and chemical resistance. Some amorphous polymers, polyethersulphone (PES) and polyetherimide (PEI), were commonly used in the aerospace industry but they were replaced with semi-crystalline polymers such as polyetheretherketone (PEEK) and polyphenylenesulphide (PPS) due to low

chemical solvent resistance [23]. The mechanical properties of amorphous polymers can be found in Table 2.2.

Table 2.2 Properties of thermoplastic polymers commonly used in composite material [23]

Thermoplastics	Type	Density (g/cm^3)	Tensile modulus (GPa)	Tensile Strength (MPa)	Melting point (°C)
Polypropylene (PP)	Semi-crystalline	0.89–0.91	1.50–1.75	28–39	134–165
Polyethylene (PE)		0.918–0.919	0.15	10–18	104–113
Polyamide (PA)		1.03–1.16	0.7–3.3	40–86	211–265
Polypheylenesulphide (PPS)		1.35–1.43	3.4–4.3	28–93	280–282
Polyetherether ketone (PEEK)		1.3–1.44	3.1–8.3	90-100	340–344
Polyetherimide (PEI)	Amorphous	1.26–1.7	2.7–6.4	100-105	220
Polyethersulphone (PES)		1.36–1.58	2.4–8.62	83–126	220

Various semi-crystalline polymers are used for composite material applications because of good mechanical properties and chemical resistance compared to amorphous polymers. Polypropylene (PP) is one of the most used semi-crystalline polymers because of its good chemical resistance and low processing temperature with medium modulus and strength. PP is used for injection molding, extrusion and compression molding with short and long fibers or continuous fibers. Polyethylene (PE) has low melting temperature and its high density type (HDPE) has good toughness. Polyamide (PA), which is also called as Nylon, is one of commonly used engineering thermoplastics in many industries. PA can be divided into several kinds according to the numbers of polyethylene segments (CH_2) separated by peptide units (NH-CO) which are either parallel or antiparallel [24]. The most commonly used polyamide polymers are Nylon 6 and Nylon 6,6. PA has better mechanical properties than PP and PE with higher temperature use range due to its high

melting temperature. Polyether ether ketone (PEEK) and poly phenylene sulphide (PPS) need high processing temperature due to their high melting temperature but the mechanical properties are superior to other semi-crystalline polymers which lead to adapt them in aerospace industry.

2.1.3 Description of the Material in the Present Study

There are a lot of material combinations which can be selected for CFRP in terms of reinforcement, matrix, and manufacturing process. In the present study, short carbon fiber composite material based on Nylon 6 (Commercial name: HiFill® PA6 CF30 by Techmer PM) is selected as the material joined by ultrasonic welding technology. However, this study is not limited to the range of the material chosen. The results of the present study can be transferred to entire thermoplastic composite materials based on semi-crystalline polymers reinforced by short fibers, long fibers and even continuous fibers. In the next section, joining technologies for CFRP will be reviewed for the state of the art.

2.1.4. Joining Technologies for Carbon Fiber Reinforced Thermoplastics

Joining of composite materials including CFRP is an important issue in using them in various industries especially automotive industries [24]. Joints are generally considered as the weakest location in the assembled structure and failures often initiate from the joints. Conventional joining technologies such as mechanical fastening and adhesive bonding which are used in aerospace industries have some limitations such as stress concentration from drilling holes for mechanical fastening or laborious surface preparations for adhesive bonding [25]. Fusion bonding/welding technologies for CFRP are considered potential for thermoplastic composite joining because they don’t have the limitations of conventional joining technologies [26]. Fusion bonding technologies

use various sources for heating and generating molecular inter-diffusion of the workpieces to be joined at their interface [6]. Spin welding, vibration welding, ultrasonic welding, induction welding, microwave heating, dielectric heating, resistance welding, focused infrared welding and hot gas welding are common fusion bonding technologies in various industries [5]. The comparison of fusion bonding technologies can be found in Table 2.3.

Table 2.3 Comparison of fusion bonding technologies for thermoplastic composites [5]

Fusion bonding process	Heating time	Specific parameters	
Spin welding	1-20 s	Rotational speed	1-20 m/s
Vibration welding	1-5 s	Frequency	100-240 Hz
		Amplitude	1-5 mm
		Pressure	1-4 MPa
Ultrasonic welding	3-4 s	Frequency	20-40 kHz
Induction welding	10 s to 6 min	Frequency	60 Hz-100 MHz
Microwave heating		Frequency	1-300 GHz
Dielectric heating		Frequency	1-100 MHz
Resistance welding	30 s to 5 min	Power input	30-160 kW/m^2
		Pressure	0.1-1.4 MPa
Focused infrared welding	30 s	Beam temperature	650 °C
Hot gas welding		Gas flow	15-60 l/min
		Temperature of gas	200-300 °C

2.2. Theoretical Background of Ultrasonic Welding Technologies for CFRP Joining

Ultrasonic welding technology is one of the most promising joining technologies in high volume production industry for thermoplastic composite materials due to its short cycle time and good adaptability for automation. Ultrasonic welding process uses low amplitude (1 ~250 μm)

mechanical vibrations of the horn at very high frequency (10~70 kHz, generally 20~40 kHz). The bonding mechanism of ultrasonic welding for metals is solid-state metallic adhesion or bonding at a thin interface layer of two workpieces. On the other hand, ultrasonic welding for polymers is based on a fusion bonding mechanism. The vibration directions of horn are different for ultrasonic welding for polymers and metals due to the different bonding mechanisms. Vibrations parallel to the work-piece surface are used for joining metals and vibrations normal to the work-piece surface are used for joining polymers [27].

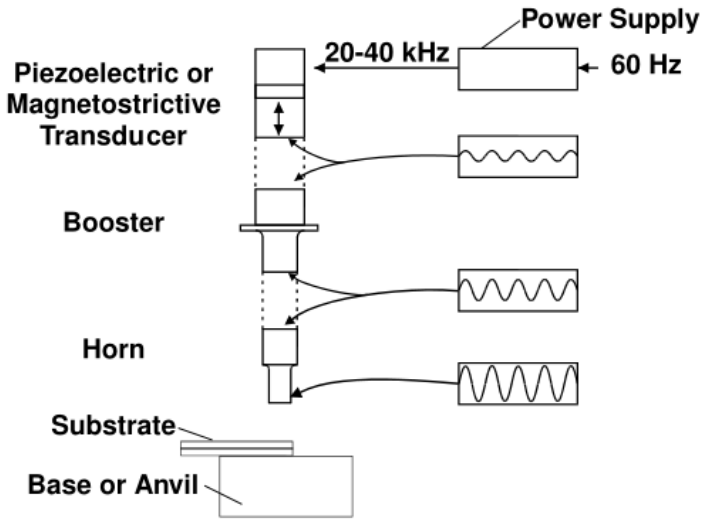

Figure 2.2 Schematic diagram of an ultrasonic welding device [5]

A machine for ultrasonic welding of polymers consists of a power supply, a transducer, a booster and a horn which are shown in Figure 2.2 [5]. The power supply converts low voltage electricity of 50 - 60 Hz to high-frequency (20 - 40 kHz). The transducer converts the electrical energy from the power supply to the mechanical vibrations via piezoelectric ceramic crystals. The booster controls the amplitude of the mechanical vibrations of the converter and transmits

vibrations to the horn. The horn can be made of titanium, steel, or aluminum and conveys mechanical vibrations to the workpieces [8].

The ultrasonic welding process can be divided into five sub-processes: (1) mechanics and vibrations of the parts, (2) heat generation, (3) heat transfer, (4) flow and wetting, and (5) intermolecular diffusion [9]. In this section, the heating mechanism and process parameters for ultrasonic welding will be reviewed.

2.2.1. Heating Mechanism of Ultrasonic Welding

Ultrasonic welding process uses small amplitude of high frequency vibrations to generate heat. The heating mechanism of ultrasonic welding can be divided into two frictional movements which are interfacial friction and intermolecular friction.

Intermolecular Friction

Viscoelastic materials such as polymers have storage modulus which represents their elastic behavior and loss modulus E'' which represents their viscous behavior. These behaviors depend on temperature and time. Thermoplastic composite materials which have viscoelastic behaviors generate heat when they are subjected to cyclic loading due to their energy dissipation via their viscous behavior by intermolecular frictions in their molecular structures [9, 28]. The loss modulus is related to the energy dissipation and the energy dissipation is transferred to heat as shown in Figure 2.3.

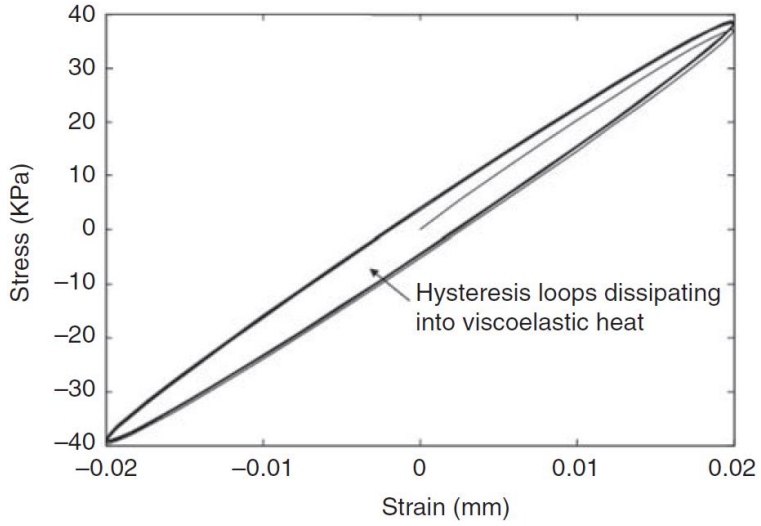

Figure 2.3 Stress–strain curve under ultrasonic vibration [30]

Tolunay et al. showed the heating and bonding mechanism of ultrasonic welding for polystyrene as a combination of bulk heating and interface heating experimentally [29]. Benatar et al. explained the heating mechanism with the intermolecular friction heating experimentally and analytically for ultrasonic welding of PEEK graphite composite material [9]. He measured viscoelastic properties of material with using Dynamic Mechanical Analysis - DMA machine and shifted the viscoelastic properties by using time-temperature superposition to get the viscoelastic properties at high frequency. The Equation 2.1 shows the heat generation from viscoelastic energy dissipation via intermolecular friction. Other many researchers adapted this heating mechanism for studying ultrasonic welding process.

$$\dot{Q}_{intermolecular\ friction} = \alpha_h^2 \frac{\omega \varepsilon_0^2 E^{"}}{2} \qquad \text{(Eq. 2.1)}$$

where α_h is hammering correction factor, ω is vibration frequency, ε_0 is strain, and $E^{"}$ is loss modulus.

However, the intermolecular friction heating is not the only heating mechanism of ultrasonic welding of CFRP and there is another heating mechanism that many researchers have ignored due to relatively small contributions for heating within the cases of small initial contact area of workpieces to be joined.

Interfacial Friction

Vertical vibrations in ultrasonic welding process are transferred to horizontal deformation at the interface of workpieces due to the boundary conditions. The horizontal deformation accompanies with slippage and friction at the interface. The friction will generate heat at the rough surfaces of work pieces, generally at the energy directors which have less stiffness than workpieces themselves to be led to energy concentration [26].

Many researchers have ignored the interfacial friction heating because the amount of heating is not very significant. Recently Zang et al. revealed that the interfacial friction heating is dominant from room temperature to the glass transition temperature of materials rather than other heating mechanism [30]. And Vilegas showed interfacial friction drives the heating process at early stage of ultrasonic welding process experimentally [31]. The two studies use rectangular shape of energy directors which have large contact area at the beginning of ultrasonic welding process. And this means that the case of ultrasonic welding without energy directors should consider the interfacial friction heating important. The interfacial friction heating rate can be calculated with below equation.

$$\dot{Q}_{interfacial\ friction} = \alpha_h^2 \omega \mu |\sigma^*_{normal} \delta u^*| / \pi \qquad \text{(Eq. 2.2)}$$

where α_h is hammering correction factor, ω is vibration frequency, μ is friction coefficient, σ^*_{normal} is the normal stress on the horizontal interface, and δu^* is the horizontal displacement discontinuity across the interface.

2.2.2. Process Parameters in Ultrasonic Welding

There are many studies regarding ultrasonic welding process parameters such as trigger force, welding energy/power (time), holding time, amplitude (or amplitude percentage), and welding speed et al. Many researchers have conducted their work to reveal the influences of process parameters on the performance of ultrasonic welding [32-35].

Initially full factorial experiments were conducted to study the effect of process parameters [32]. Taguchi method was also used to find out the effect of various process parameters. The results show that weld time and amplitude of vibration are the most important factors. The optimized process parameters generate the highest weld strength. But this study cannot explain the large range of weld strength for same process parameters [33-35].

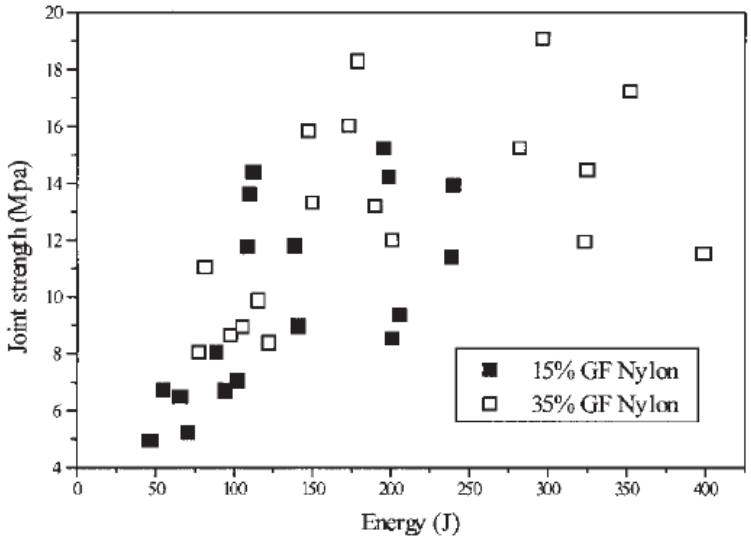

Figure 2.4 Variation of joint strength with energy dissipation in the ultrasonic welding of thermoplastic composites [35], the materials have 15% and 35% weight fraction of glass fiber with nylon.

2.2.3. Energy Directors

Among existing assembly methods, ultrasonic welding remains the most efficient method for CFRP joining due to its robustness and short cycle time. But in most cases of ultrasonic welding of CFRP, energy directors which have narrow cross section to induce melting are used for improved weldability. Many researchers conducted their work on energy directors for ultrasonic welding experimentally [35-39]. Liu and Chang [35] optimized the ultrasonic welding process and the shape of energy directors using design of experiments and found that semi-circular energy directors provided the highest weld strength with optimized process parameters. Villegas and Bersee [36] conducted investigations on the effect of energy director location and its density for the weld area and lap shear strength. Villegas et al. [37] suggested a rectangular energy director provided as a form of film and compare flat energy directors and triangular energy directors in terms of heat generation. In the same way, the thickness effect of flat energy directors on ultrasonic

welding was shown by Palardy and Villegas [38]. Chuah et al. [39] investigated the shape effect of energy directors for thick workpieces of 30mm which have far field ultrasonic wave propagation. These works were done with the workpieces with energy directors which are consisting of polymers without reinforcements and supplied by additional process such as hot stamping or film form. It is not efficient for industry to have energy directors due to the additional cost and process cycle time. The study of ultrasonic welding process without energy directors is necessary to find out the heat generation phenomena and process parameters' influence on heat generation.

There is limited research on the ultrasonic welding of composite materials without an energy director. Wang et al. investigated the influence of the process parameters of ultrasonic welding without energy directors on the weld strength of Nylon 6-based CFRP [10, 11]. Weld attributes were investigated with various process parameters and the relationship between weld attribute and weld strength was shown in ultrasonic welding of CFRP without energy directors [10]. A FEM model was created to predict weld strength based on weld attributes [11]. However, their studies showed large variations in weld strength—even when process parameters were kept constant—and relatively lower average values compared to the strength of the base CFRP.

Luo et al. proposed the use of external thermal or chemical sources during ultrasonic welding without energy directors to promote bonding between two surfaces [51]. The main application of these methods is microbonding of Polymethyl methacrylate (PMMA), which produces low-strength welds. These methods are not suitable for joining large components for which the weld strength must reach very high values (between 2 kN and 4 kN).

Li et al. suggested a blank holder to focus the welding under horn and their study showed that the blank holder with critical release time increases the weld strength but the variation of weld

strength is still large [52]. This variability may be explained by the instability of weld formation and consolidation, as well as surface waviness produced when preprocessing the workpieces.

Hence, there is a strong need to investigate on material characteristics which can influence on the welding process and the heating phenomenon in ultrasonic welding process without energy directors and to improve the weld quality.

2.2.4. Differences between Bonding Mechanisms in USW with and without Energy Directors

The difference between the bonding mechanisms of USW with and without energy directors is mainly in initial stages of process (Surface contact and wetting stages). A schematic representation of contact initiation and propagation for USW with and without energy directors is presented in Figure 2.5.

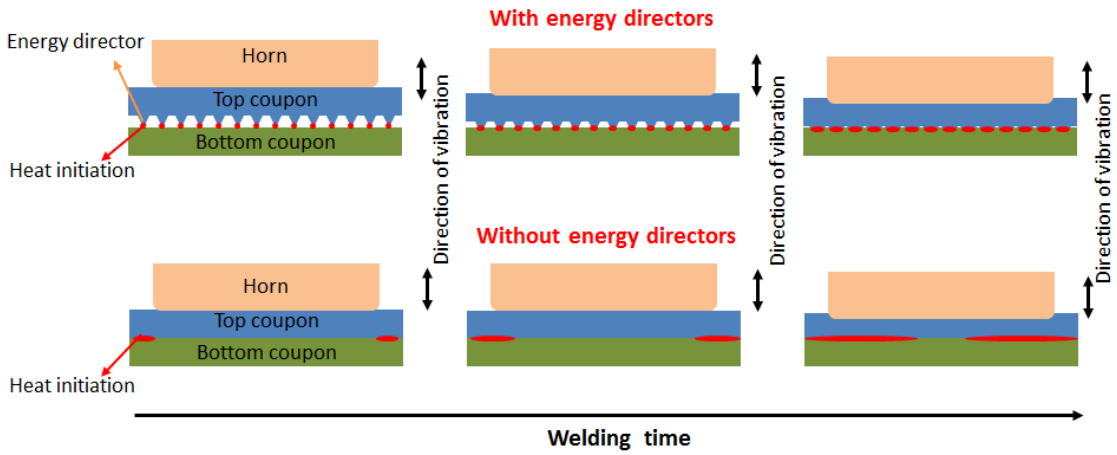

Figure 2.5 Heat generation and flow propagation toward weld formation in USW with and without energy directors

This difference is caused by an initial discontinuous contact surface between energy directors (built in on the surface of the upper coupon) and the bottom coupon in the case of USW with

energy directors and almost full contact between the two coupons in the case of USW without energy directors. Owing to localized contact between the energy directors and bottom coupon, the wetting step is reached faster compared to nonlocalized contact (theoretical infinite contact) in the case of no energy director. Moreover, the high speed camera recording of USW without energy directors shows that contact is initiated on a circumferential area under the horn leading to weld formation.

It should be noted that the main differences between the two processes are in the initiation and propagation directions of intimate contact, which strongly depends on the uniformity of the workpiece's structure in the superficial layer and workpiece flatness (or roughness). These two attributes of coupons are determined during injection molding, and they generally depend on the degree of crystallinity and the distribution of fibers.

2.2.5. Environmental Conditions

Ultrasonic welding performance depends on the process parameters but also on the mechanical properties of material which are bonded. For thermoplastic composite materials, temperature and moisture are critical parameters for the performance of ultrasonic welding.

Zhi et al. shows the effect of moisture on the performance of Nylon 66 and carbon fiber composite materials. This study presents that the moisture affects the mechanical properties of materials which leads to the change of ultrasonic welding performance due to the easy water absorption characteristic of Nylon 6,6 [40].

Wang et al. suggested the interfacial preheating method to improve the weld strength [41]. This study can induce the early intermolecular friction heating via preheating which leads to

improvement of weld strength for high welding energy cases. But it doesn't show the fundamental reasons of temperature effects on ultrasonic welding process.

2.3. Modeling of Ultrasonic Welding

Ultrasonic welding is a complex process and many processing parameters are included during the welding process. To test the sensitivity of the processing parameters on welding quality, one can either perform a series of welding experiments changing values of the processing parameters, or develop a model for simulating the process. Actually, process modeling can speed up the investigation and optimization of new processes since a variety of processing conditions can be assessed in a short time. Moreover, in the simulation, the process is investigated without any expenses in raw materials or experimental set-up or tooling, thus reducing the cost of the process development. Hence, many studies have been carried out on the modeling of the ultrasonic welding process.

2.3.1. Modeling for Ultrasonic Welding Process for CFRP

Wang et al. [42] investigated the temperature field change in energy directors of PEEK and CFRP through FEM. Suresh et al [13] showed temperature distribution in various energy directors such as triangular, rectangular, and semicircular shapes in near and far field. Levy et al. [44] investigated the USW process with triangular energy directors influenced by amplitude of vibration, holding force, thickness of specimen, radius of curvature at the tip of energy directors, and angle of energy directors in 2D numerical model. Levy et al. [45] also made a numerical model to investigate physical mechanisms in ultrasonic welding process with flat energy directors. In the same way, there are few papers for the modeling of ultrasonic welding process without energy

directors. The heating phenomenon without energy directors is different because there is no stress concertation at the energy directors.

Levy et al. [46] used time homogenization techniques to reduce the simulation time via homogenizing two separated time steps which are vibrations and flows of molten polymer. This allowed a lot of time saving for the simulation of ultrasonic welding process but this study doesn't result in accurate results as direct calculation depends on time scale factors.

Tutunjian et al. [68] introduced a FEM model with Differential Ultrasonic Spot welding (DUS) and showed that the frictional heating mechanism initiated for the case of different contact area from the horn and the anvil. However, material properties in the FEM model were not measured temperature dependently and the heating phenomena was not shown clearly. In the same way, there are few papers for the modeling of USW process without energy directors. The heating phenomenon without energy directors is different because there is no stress concertation in energy directors. The same research group presented a 2D explicit FEM model to demonstrate the temperature distribution and evolution during USW process recently [75].

2.3.2. Dynamic Response Analysis of Ultrasonic Welding

The dynamic response of vibration system in ultrasonic welding needs to be considered due to the high frequency oscillation for heat generation. For ultrasonic welding for metallic materials, there has been some researches for the dynamic response using a discrete model of single degree of freedom mass-spring-damper system.

Kang et al. investigated the dynamic response and the dynamic stress in ultrasonic welding of copper and aluminum [47-48] by providing analytic solutions of simplified welding systems. The same research group also calculated the vibration energy loss due to damping considering the

resonance at the natural frequency of vibration systems [49]. Kim et al. used three methods such as a discrete model of single degree of freedom model, a continuous model of multi degree of freedom cantilever beam, and a FEM model based on real-world applications [50]. These researches showed the important role of dynamic analysis according to the locations of welding and the vibration system structure in ultrasonic welding to predict the welding performance. However, these researches are for ultrasonic welding of metallic materials. Therefore, the study of dynamic analysis of ultrasonic welding of CFRP is still necessary.

Chapter 3 Influence of Morphological Parameters on Welding Process and Weld Performance of CFRP by Ultrasonic Welding

Ultrasonic welding (USW) without energy directors is one of the most efficient joining technologies for carbon fiber reinforced plastics (CFRP). However there is limited research on the USW of CFRP without energy directors even though it has been realized that the performance of such weld is low and unstable. The origin of this poor weld performance can be associated with changes in the material behavior in the presence of heat generated through USW combined with the fiber distribution in the weld area. In the case of the thermoplastic materials used as a matrix, the volume fraction of the crystalline phase influenced by heating and cooling during the prior manufacturing process determines the material's viscoelastic behavior [53, 54]. All of these influences the weld performance must be investigated in order to achieve stable USW performance and the USW without energy directors are influenced more than the case with energy directors.

In this chapter, the impact of morphological parameters, such as the degree of crystallinity (DoC) and the ratio of α and γ crystalline phases (α/γ ratio), on the performance of USW for CFRP with Nylon 6 matrix are analyzed using single lap shear tests. To understand the role of the short carbon fibers in the weld formation, pure Nylon 6 is used as a reference in these experiments. To induce variation in the morphological parameters of the CFRP workpieces, different heat treatments are applied to the workpieces before welding. These heat treatments are called annealing processes, analogously with metal annealing processes. The morphological parameters are measured after annealing and compared with their values before annealing (as-received). Annealed and as-received workpieces are welded, then their weld performances are measured

through single lap shear tests. Thus, the influences of morphological parameters are analyzed through a comparison of the joint performances of annealed and as-received workpieces.

Section 3.1 describes materials used in the experiments; Section 3.2 introduces morphological parameters; Section 3.3 explains the experiments used to measure morphological parameters, mechanical properties, weld strength, and ultrasonic welding procedures; Section 3.4 discusses the relationship between welding performance and morphological parameters; and Section 3.5 summarizes and concludes the chapter.

3.1. Materials

The materials used in this research are HiFill PA6 CF30 and HiFill PA6 (Techmer PM, Tennessee, USA). HiFill PA6 CF30 is a CFRP with a Nylon 6 matrix. The CFRP has a 30% weight fraction of short carbon fiber. HiFill PA6 is a pure Nylon 6 used for comparing and investigating the influence of carbon fibers on weld formation.

The workpieces for USW are manufactured by injection molding with HiFill PA6 CF30 pellets. Their glass transition temperature (T_g) is 60°C and their melting temperature (T_m) is 220°C. The pellets were dried at 80°C for 4 hours to reduce the moisture to less than 0.12%. After injection molding, the workpieces were kept dry in a sealed plastic bag. The dimensions of the molded workpieces were 127 mm × 38 mm × 3 mm.

The matrix of the CFRP is Nylon 6, which is a semi-crystalline thermoplastic polymer with amorphous and crystalline phases. The crystalline phase of Nylon 6 has two forms—α and γ (Figure 3. 1)—which have different structures and properties. The α form has a higher Young's modulus and stability than the γ form. The α form has monoclinic structure and is generated with a relatively high-temperature crystallization process with a slow cooling rate. The γ form has a

hexagonal or pseudo-hexagonal structure and is generated with a relatively low-temperature crystallization process with a rapid cooling rate [55]. Their different mechanical and physical properties are shown in Table 3.1. Figure 3.1 shows the two crystalline forms of Nylon 6. The γ form can be transformed into the α form by treatments such as annealing and stretching [55, 56].

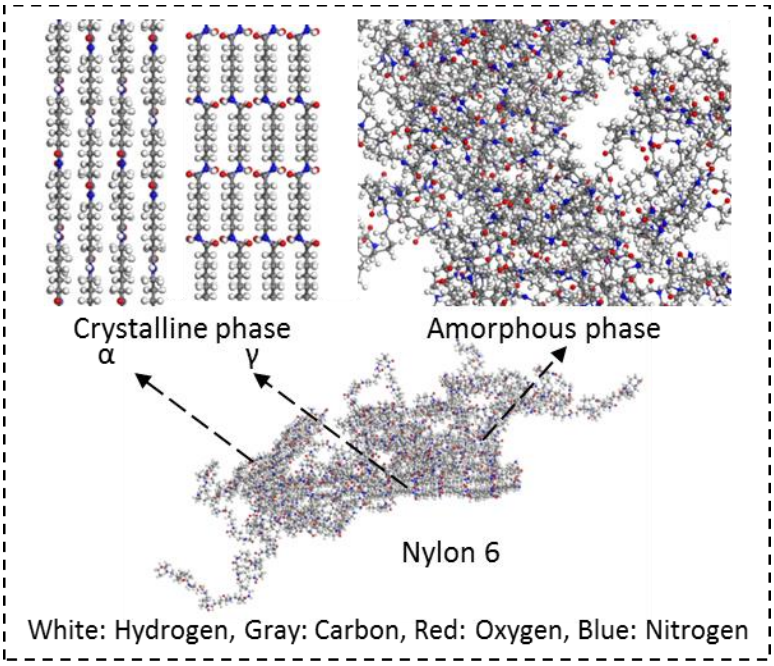

Figure 3.1 Structure of Nylon 6

Table 3.1 Mechanical and physical properties of α and γ crystalline forms [55, 56]

Property	α form	γ form
Crystal structure	Monoclinic	Hexagonal/pseudo-hexagonal
Lattice constants	a = 9.587 Å b = 17.602 Å c = 7.760 Å β = 69°	a = 4.931 Å b = 17.267 Å c = 8.810 Å β = 126.8°
Density (g/cm3)	1.23	1.16
Heat of melting, $\Delta \mathbf{H}_{\boldsymbol{m}}^{\circ}$ (J/g)	241	239
Young's modulus (GPa)	235.29	131.97

The weight fraction of the crystalline phase over the amorphous phase and the ratio of the two crystalline forms influence the mechanical and physical properties of the semi-crystalline polymer. The quantitative influence of weight fraction and ratio on the mechanical properties of the material is presented in the next section.

3.2. Morphological Parameters

3.2.1. Degree of Crystallinity (DoC)

The DoC is the percentage of crystalline phase in a semi-crystalline polymer. For Nylon 6, the DoC is the sum of the percentages of α and γ forms over the total (composed of the amorphous and crystalline phases). The DoC influences the stiffness, hardness, and heat resistance of the material. For example, a higher DoC indicates a stiffer material [53]. The DoC of a melt polymer is determined by the cooling rate used in crystallization (i.e., a slower cooling rate leads to a higher DoC).

3.2.2. Ratio of the Crystalline Forms in Nylon 6 (α/γ Ratio)

The ratio of α and γ forms in the crystalline phase is determined by the cooling rate in the crystallization step. Since these two crystalline forms have different mechanical and physical properties, changing the relative amount of each crystalline form also changes the mechanical and physical properties of the material. A higher α/γ ratio indicates that there are more α form crystals than γ form crystals in the crystalline phase of Nylon 6 and the mechanical and physical properties of the material are comparatively closer to those of the α form crystalline phase.

The DoC and α/γ ratio can differ for semi-crystalline polymers according to the process conditions, even those made using the same raw materials. Furthermore, materials that have the same DoC may vary in α/γ ratio based on process conditions.

3.3. Experimental Methods

3.3.1. Annealing Process

By analogy with metals, annealing is applied to a CFRP. In annealing, slow heating and cooling rates are used to remove the heat history of the material, carried from prior manufacturing processes such as injection molding [55]. Different combinations of heating and cooling rates generate different DoCs and α/γ ratios [55, 57-58]. In this research, annealing is conducted with various annealing temperatures (80-180°C with increments of 20°C) and applied to the CFRP workpieces before USW. A Blue M furnace (Lindberg/MPH, MI, USA) is used for annealing. The heating and cooling rates for annealing are 10°C/h. Between the heating and cooling stages, the workpieces are maintained at the annealing temperature for 2 hours. After annealing, the workpieces are stored in sealed bags to prevent moisture absorption. In the next sections, these annealed workpieces are tested against non-annealed (or "as-received") workpieces.

3.3.2. DoC Measurement by Differential Scanning Calorimetry (DSC)

A Discovery DSC machine (TA Instruments, DE, USA) is used to measure DoCs. The weight of the DSC samples is about 10 mg and data are collected from nine different locations on the workpiece after injection molding for both the annealed and as-received samples, as shown in Figure 3.2.

Figure 3.2 Top view of the CFRP workpiece: Showing the locations of the nine samples cut from the workpiece and used for DSC

In DSC, the samples are heated from 25°C to 270°C at a rate of 10°C/min, kept for 5 min at 270°C, and cooled to 25°C at a rate of 10°C/min (Figure 3.3).

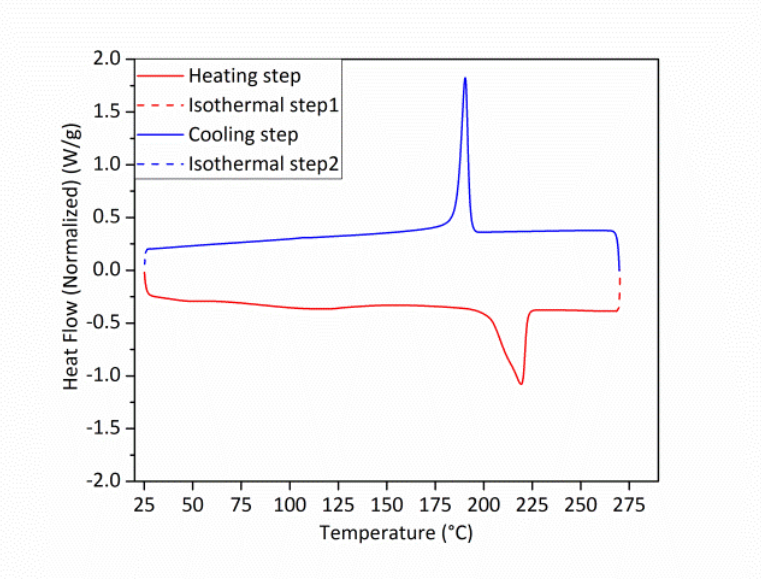

Figure 3.3 Heat flux in the DSC experiment: The DoC is determined by the integration of the heat flux in the heating step.

The DoC is calculated from the heating cycle using the following equation:

$$DoC_{DSC}(\%) = \frac{\Delta H_m}{(1-w_f)\Delta H_m^0} \times 100 \qquad \text{(Eq. 3.1)}$$

where ΔH_m is the melting enthalpy of the samples as measured during the heating cycle, w_f is the weight fraction of short carbon fibers (in this research, 0.3), and ΔH_m^0 is the melting enthalpy of the 100% crystalline form of Nylon 6 (240 J/g) [59].

3.3.3. Measurement of the α/γ Ratio by X-Ray Diffraction (XRD)

XRD is used to investigate the structure and the morphology of the material [59]. A Miniflex X-ray diffractometer (Rigaku Americas Corporation, TX, USA) is used to obtain the X-ray diffraction patterns, which are used to calculate the fraction of constituent crystalline forms in the material. The XRD scan speed is 1°/min and the diffraction angle (2θ) ranged from 10° to 30°. A Cu Kα metal target is used and the voltage and current are 30 kV and 10 mA, respectively. XRD measurements are conducted for the annealed and as-received workpieces from specimens prepared by cutting the workpieces from the position where USW was performed. The dimensions of the specimens are 9 mm × 9 mm × 3 mm (Figure 3.4). From the completed XRD measurements, the peak curves are obtained according to diffraction angle (Figure 3.5).

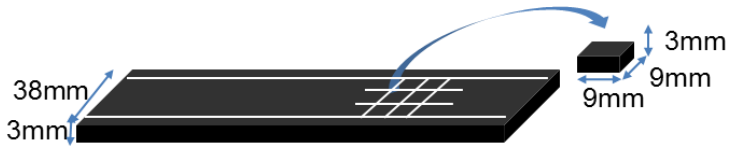

Figure 3.4 Dimensions of injection molded base materials and collection of XRD specimens

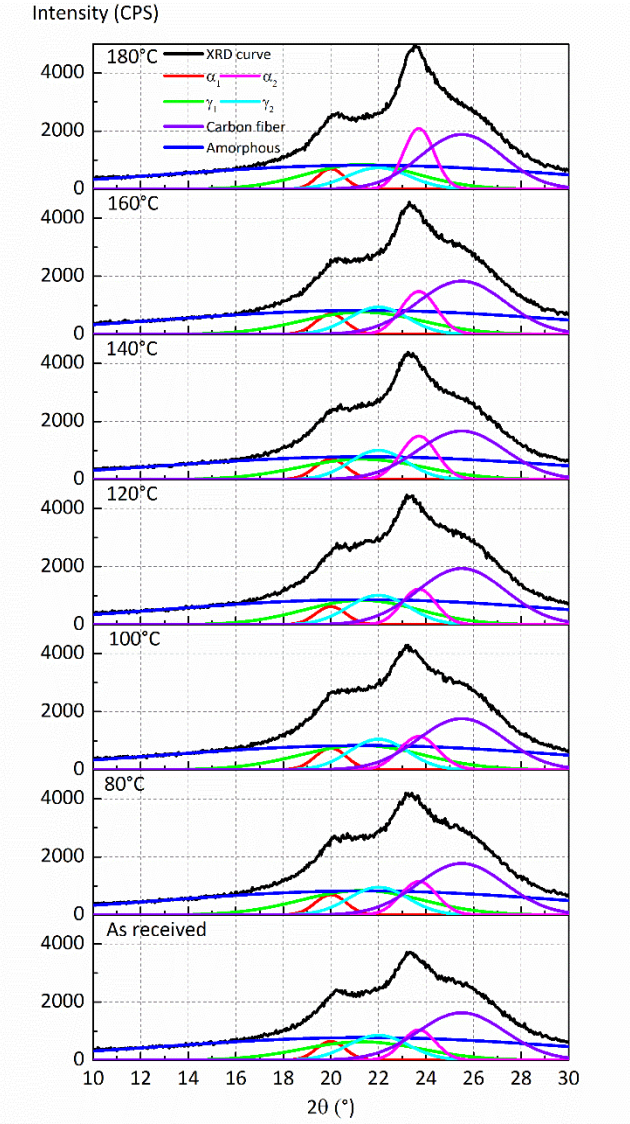

Figure 3.5 XRD curves and their deconvolution for the as-received and annealed CFRP. Two peaks (at 20° and 23.7°) corresponding to the α crystalline phase are clear. Two peak (at 21.3° and 22°) corresponding to the γ crystalline phase cannot be seen clearly.

XRD pattern data were obtained from the completed measurements according to diffraction angles. The XRD pattern data were fit to curves using the adjacent averaging method based on 20 data points from the original experimental data (Figure 3.5). The background of XRD curves was not removed for the deconvolutions of the XRD curves because the randomly oriented polymers in the amorphous phase were included the background in all regions of the XRD curves between

$2\theta = 10°$ and $30°$. Each phase of the CFRP contains 2θ locations. The peaks at $2\theta \approx 20°$ (α_1) and $23.7°$ (α_2) represent the α forms. The peaks at $2\theta \approx 21.3°$ (γ_1) and $22°$ (γ_2) represent the γ forms [55, 59-61]. The peak of carbon fibers is at $2\theta \approx 25.5°$ [61]. The peak of the amorphous phase is at $2\theta \approx 21.43°$ [55]. Each peak curve was calculated using a Gaussian shape model with manual adjustments of the heights and widths of peaks at the beginning to provide reasonable starting points. The agreement between experimental data and the prediction obtained from the Gaussian shape model satisfied the yielding coefficients of determination (R^2) above 0.98. The curve fitting functions in the Origin data analysis software were used to calculate the area under the curves for each peak (A_{α_1}, A_{α_2}, A_{γ_1}, A_{γ_2}, A_{amorpous}, $A_{\text{carbonfiber}}$). The fractions of the α phase (X_α) and γ phase (X_γ) and the α/γ ratio were calculated from the equations given below (Equations 3.2-3.4).

$$X_\alpha = \frac{A_{\alpha_1} + A_{\alpha_2}}{A_{\alpha_1} + A_{\alpha_2} + A_{\gamma_1} + A_{\gamma_2} + A_{amorphous}} \quad \text{(Eq. 3.2)}$$

$$X_\gamma = \frac{A_{\alpha_1} + A_{\gamma_2}}{A_{\alpha_1} + A_{\alpha_2} + A_{\gamma_1} + A_{\gamma_2} + A_{amorphous}} \quad \text{(Eq. 3.3)}$$

$$\alpha/\gamma\ ratio = X_\alpha / X_\gamma \quad \text{(Eq. 3.4)}$$

3.3.4. Measurement of Viscoelastic Properties by Dynamic Mechanical Analyzer (DMA)

The viscoelastic properties of CFRP represent their behavior under dynamic loading; these properties are related to intermolecular heating during USW [30, 31, 45, 62, 63]. Viscoelastic properties, such as storage modulus (E′) and loss modulus (E"), can be measured using a DMA [57, 58]. The glass transition temperature is calculated from the relationship between the storage and loss moduli.

A DMA machine (TA instruments, DE, USA) is used to measure the storage and loss moduli with a three-point bending fixture. The DMA specimens have dimensions of 10 mm × 37 mm × 1 mm dimensions and the span length of the fixture is 25 mm. The specimens are obtained from cutting and softly sanding of workpieces made by injection molding. The frequency–temperature sweep method is used in a temperature range of 25–80°C and frequency range of 0.05–10 Hz. A convection-controlled heating chamber is used to stabilize the temperature, with a soaking time of 300 s before dynamic loading.

3.3.5. Ultrasonic Welding Process

An IQ Servo USW machine (Dukane, IL, USA) is used for USW at a vibration frequency of 20 kHz. A 9.5-mm-diameter circular horn is used to weld the workpiece samples. Lap joint bonds are made with a 12.7 mm × 12.7 mm overlap area after CNC milling the edge region to prevent edge welding (Figure 3.6). The milling depth is 0.5 mm (16% of the workpiece's thickness). The other processing parameters are a welding speed of 0.25 mm/s, trigger force of 150 N, amplitude of 50 µm, and holding time of 3 s.

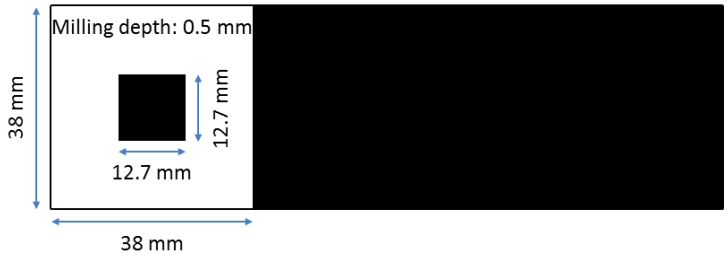

Figure 3.6 Overlap area of workpieces to prevent the edge welding (12.7 mm x12.7 mm)

3.3.6. Temperature Measurement in USW

USW generates heat at the interface between the workpieces to be welded. However, there is no standard method for measuring the temperature at the interface. In this research, 0.13-mm-diameter Type K thermocouples (OMEGA, Egham, UK) with a maximum temperature threshold of 593°C is placed at the interface of the welding area as shown in Figure 3.7. The thermocouple is triggered with the USW process, so that the start of their recordings corresponds to the initiation of the ultrasonic effect. Data are recorded using an Arduino development board with an increment of time of 0.01 s. The temperature is recorded during the welding of five annealed and five as-received workpieces.

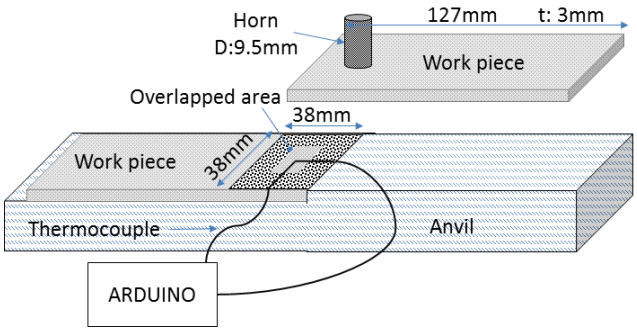

Figure 3.7 Experimental setting for temperature measurement during USW process

3.3.7. Measurement of Weld Strength

Single lap shear tests were conducted on the welded coupons using a 3300 series universal test machine (Instron, MA, USA) with a 5 kN load cell at a test speed of 2 mm/min. The set-up for the single lap shear tests is shown in Figure 3.8(a). In the tests, the loading direction was tilted because of the horizontal gap between the upper and lower fixtures. The maximum load divided by the overlapped area ($A_{Overlap}$) during the test was used to evaluate weld strength (τ) shown as Equation 3.5.

$$\tau = F_{interface}/A_{Overlap} = F_{loading}cos(\alpha)/A_{Overlap} \qquad \text{(Eq. 3.5)}$$

A digital image correlation system (DIC) was used to collect titling data during the single lap shear tests. The tilting angle was calculated from the initial position of specimens at the beginning of the tests. The maximum titling angle during the tests was below 5°. For this tilting angle, $\cos\alpha$ in Equation 3.5 was 0.9962. This shows that the tilting during the lap shear tests is negligible. The tilting angle distribution immediately before the break in the single lap shear tests is shown in Figure 3.8(a) and the evolutions of the tilting angle for the five replicates are shown in Figure 3.8(b).

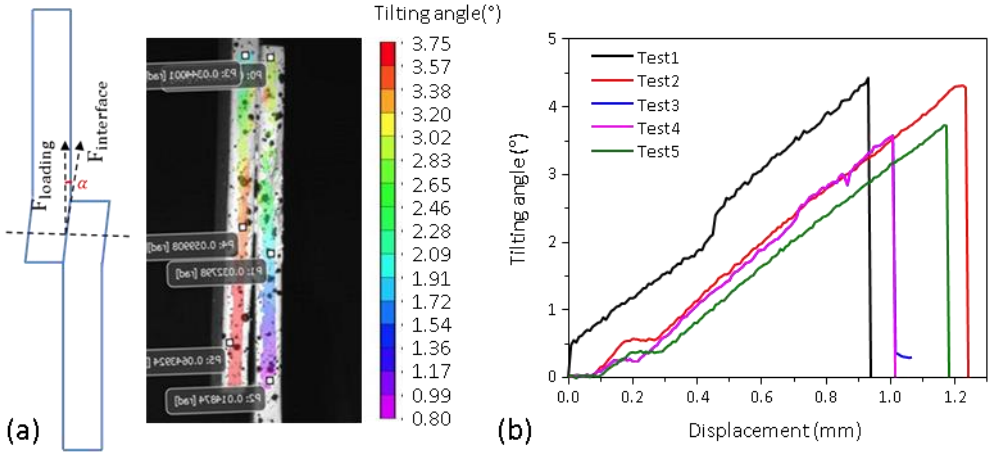

Figure 3.8 Set-up for measurement of the titling angle with respect to the loading direction: (a) DIC measurement on the lap shear configuration, (b) The plot of the maximum tilting angle

In addition to the lap shear tests, tensile tests were conducted to determine the ultimate tensile strength of the coupons. A hydraulic universal testing machine (MTS, MN, USA) with a 100 kN load cell was used to perform the tests at a speed of 2 mm/min. A minimum of five replicates were used for each test.

3.4. Results and Discussion

3.4.1. Degree of Crystallinity

DoC results measured via DSC are shown in Figure 3.9. The values of the as-received CFRP are not uniform, which means the distribution of material morphology has variation. In comparison, after annealing, the DoC values become more uniform despite that the average DoC on the workpiece surface remains almost the same. The variation of DoC as-received CFRP comes from the cooling stage of manufacturing process. Figure 3.10 shows the deflection of specimens in the cooling stage of 2 cavities injection molding process using Moldflow. The result shows that the similar trend of deflection with the DoC distribution. For this study, general polyamide 6 with fibers for injection molding material is used and the process parameters in injection molding for manufacturing as-received CFRP is applied in the Moldflow simulation.

The injection molding process by which the workpieces are manufactured unevenly distributes the crystalline structure during cooling. Annealing the base material at greater than its glass transition temperature (T_g) induces a change in the crystalline structure [60]. Pure Nylon 6 has less DoC variation compared to the CFRP, as the carbon fibers have much higher thermal conductivity than Nylon 6 does. The carbon fibers therefore speed cooling during the CFRP manufacture. These results show that annealing can control the DoC, which is one key morphological parameter.

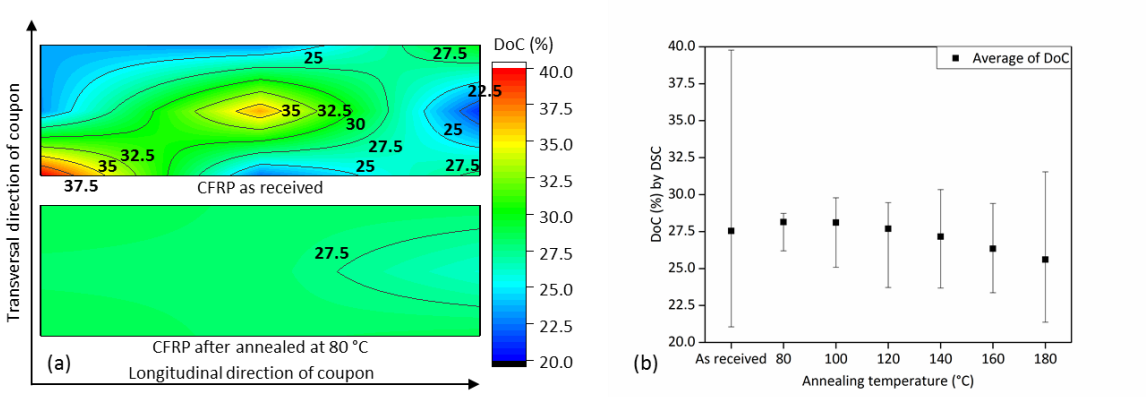

Figure 3.9 (a) DoC distribution across workpieces of CFRP as received and its changes after annealing at 80°C, (b) DoC scatters measured by DSC for CFRP as received and annealed

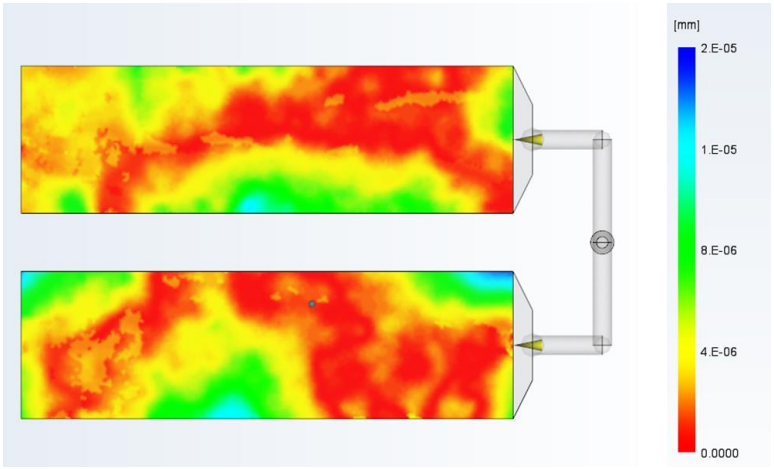

Figure 3.10 Deflection distribution in the mold at the cooling stage of 2 cavities injection molding process using Moldflow

3.4.2. α/γ Ratio

The α and γ form fractions and the α/γ ratio are illustrated in Figure 3.11. Annealing at 80°C facilitates transformation from the amorphous phase to the γ crystalline phase [60]. Annealing between 80°C and 100°C shows the same phenomenon leading to an increase of the weight fraction of the γ crystalline phase. However, between 120°C and 180 °C, significant transformation of γ crystalline phase in α crystalline phase occurs leading to another increase in the weight fraction of the α over γ [64]. Yan et al. showed that the transformation of crystalline forms differs depending on the presence or absence of carbon fibers, and that carbon fibers facilitate transformation at lower annealing temperature [61].

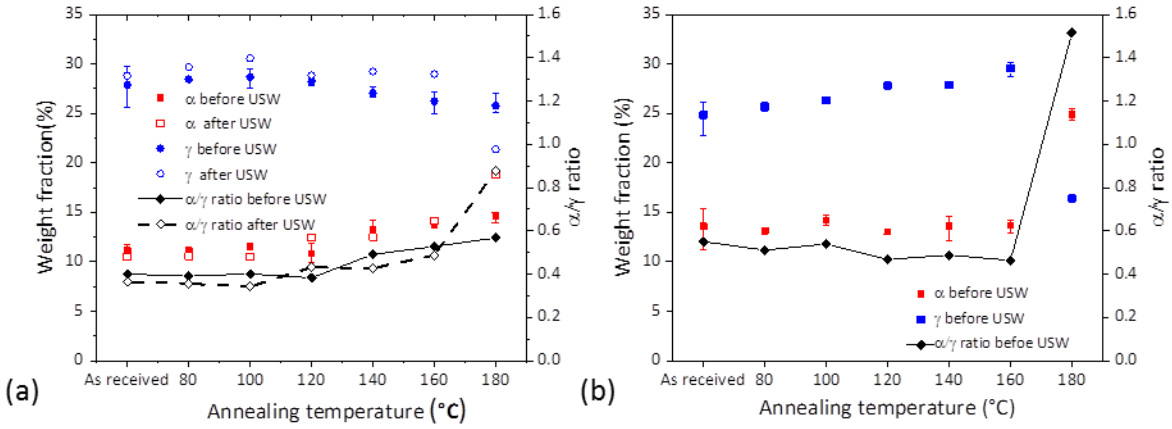

Figure 3.11 Weight fractions of α and γ crystalline forms, as well as the α/γ ratio: (a) CFRP, (b) Nylon 6 as received and annealed

The γ crystalline dominates at the surface layer of an injection molded base material, whereas the α crystalline form is dominant in its core layer [65]. Moreover, carbon fiber has a much higher thermal conductivity than Nylon 6, so it facilitates rapid cooling during injection molding, which further leads to a high weight fraction of γ form crystals. In this experiment, the measurement of

weight fraction ratio of constituents was conducted on the surface of an injection molded base material; as a result, the weight fraction of γ form crystals is higher than α form crystals in this experiment. For Nylon 6, the α/γ ratio after annealing at 180°C increase rapidly which shows easier crystalline structure change comparing to CFRP.

Measurements of the DoC and α/γ ratio with different annealing temperatures confirm that the annealing process changes the crystalline structure. Annealing results in a more uniform DoC throughout the material, and the crystalline structures generated differ according to the annealing temperature. These changes in the material's morphology alter its viscoelastic and mechanical properties. The evolution of viscoelastic and mechanical properties using the annealing process will be discussed in the following sections. The lap shear test results of USW will be shown to evaluate the changes in weld strength corresponding to the changes in morphological parameters and viscoelastic and mechanical properties brought on by the annealing process.

3.4.3. Viscoelastic Properties

The dynamic mechanical behavior of the material was investigated with a DMA test, in which sinusoidal stress was applied and the material's response was measured through strain. The delay between the stress and strain is expressed as phase angle δ. The following equations explain the relationship between stress σ, strain ε, and phase angle δ at time t [66, 67].

$$\sigma(t) = \sigma_0 sin(\omega t + \delta) \quad \text{(Eq. 3.6)}$$

$$\varepsilon(t) = \varepsilon_0 sin(\omega t) \quad \text{(Eq. 3.7)}$$

$$\sigma = \sigma_0 \, sin(\omega t) \, cos\delta + \sigma_0 \, cos(\omega t) \, sin\delta \quad \text{(Eq. 3.8)}$$

$$E' = \frac{\sigma_0}{\varepsilon_0} cos\delta \quad \text{(Eq. 3.9)}$$

$$E'' = \frac{\sigma_0}{\varepsilon_0} sin\delta \qquad \text{(Eq. 3.10)}$$

$$tan\delta = \frac{E''}{E'} \qquad \text{(Eq. 3.11)}$$

where σ_0 is the maximum stress at the peak of the sinusoidal stress, ω is the oscillation frequency, and ε_0 is the strain at maximum stress. Storage modulus E' represents the elastic behavior of the material and loss modulus E'' represents its viscous behavior.

As expressed in the preceding equations, the moduli of viscoelastic materials such as polymers are a function of time at a constant temperature or a function of temperature at a constant time. The master curve for the viscoelastic properties of a polymer can be predicted using the time–temperature superposition method, in which several sets of frequency sweep results at various temperatures are used to make the master curve. This method is used to predict the viscoelastic properties for conditions which are not available to be measured experimentally. Here, the material's viscoelastic properties are predicted with a temperature sweep of 20 kHz (the USW vibration frequency). The WLF equation was used to calculate the shift factor of the master curve [67].

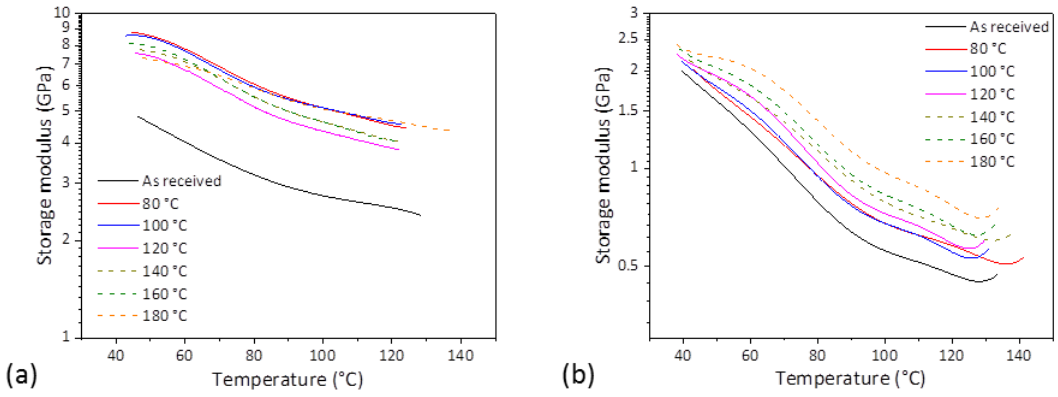

Figure 3.12 Storage modulus at 20 kHz: (a) CFRP, (b) Nylon 6 as received and annealed

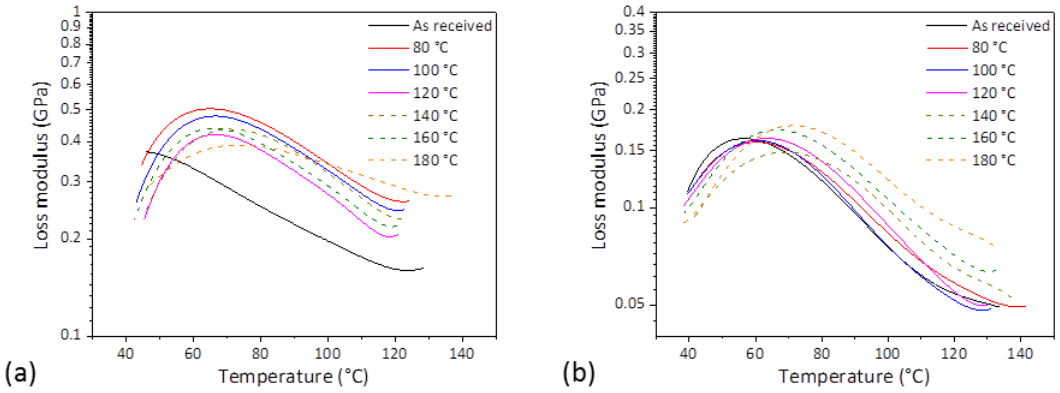

Figure 3.13 Loss modulus at 20 kHz: (a) CFRP, (b) Nylon 6 as received and annealed

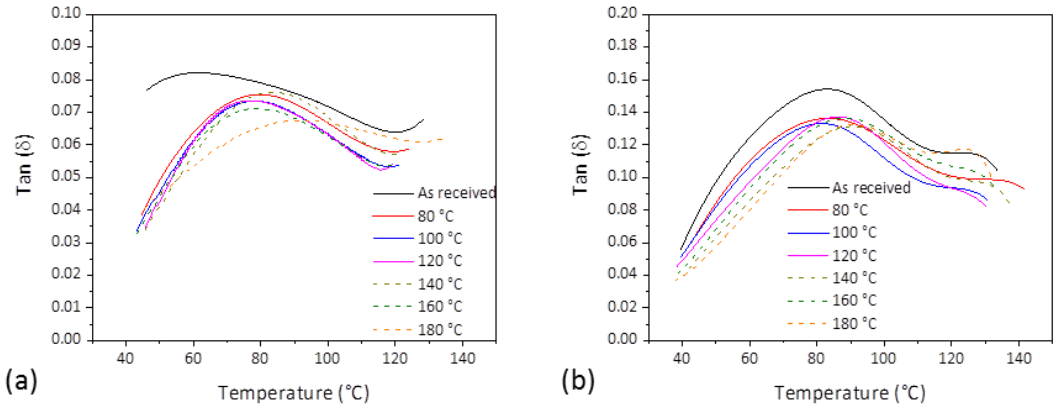

Figure 3.14 tanδ at 20 kHz: (a) CFRP, (b) Nylon 6 as received and annealed

Figure 3.12, Figure 3.13 and Figure 3.14 show the storage modulus, loss modulus and $tan\delta$ of the as-received and annealed workpieces, respectively. The storage modulus decreased with increasing temperature (Figure 3.12(a)), but was increased by the annealing process because of the crystalline structure change resulting from the annealing. The loss modulus also increased at temperatures greater than the glass transition temperature of Nylon 6 (Figure 3.13(a)). This tendency is also shown in Nylon 6 (Figure 3.12(b), Figure 3.13(b)). The apex of tanδ corresponds to the glass transition temperature of thermoplastic polymer (Figure 3.14 (a), (b)). The as-received

sample had the lowest glass transition temperature and the sample obtained after annealing at 180°C had the highest glass transition temperature. Hence, the glass transition temperature of the material increased with the annealing temperature. These results influenced the heat generation in the USW process.

At temperatures less than the glass transition or melting temperatures, the interfacial friction heating mechanism is dominant; at temperatures greater than the glass transition or melting temperatures, the intermolecular friction heating mechanism becomes dominant in the USW process [30, 41, 45, 62]. Equation 3.12 and Equation 3.13 calculate the heat flux from interfacial and intermolecular friction.

$$\dot{Q}_{interfacial\ friction} = \alpha_h^2 \omega \mu |\sigma^*_{normal} \delta u^*| / \pi \qquad \text{(Eq. 3.12)}$$

$$\dot{Q}_{intermolecular\ friction} = \alpha_h^2 \frac{\omega \varepsilon_0^2 E^{"}}{2} \qquad \text{(Eq. 3.13)}$$

where $\dot{Q}$ is the heat generation rate, α_h is the empirical hammering correction factor, μ is the friction coefficient, σ^*_{normal} is the normal stress on the horizontal interface, ω is the vibration frequency, and δu^* is the horizontal displacement discontinuity across the interface [45].

The equations illustrate that the increased storage modulus generates more heat during USW by interfacial friction, if the other parameters remain the same. In contrast, increasing the loss modulus generates more heat by intermolecular friction. Increased heat generation improves welding quality (before reaching temperatures at which heat degradation of the material occurs). Of the processing parameters, the welding energy is related to the total heat generation. A higher heating rate results in rapid heating with the same welding energy. Wang et al. [11] showed that higher welding energy results in greater weld strength, up to energy levels at which the material

degrades. The welding energy after the material melts is used to entangle molecules in the welded area and results in a better weld.

The viscoelastic behaviors of semi-crystalline polymer contribute differently to the heat generation for USW at various temperatures. The storage modulus of a semi-crystalline polymer is maintained up to the melting temperature and decreases dramatically thereafter, implying that interfacial friction is dominant until reaching the melting temperature. Above the melting temperature, intermolecular friction is dominant. The loss modulus of a semi-crystalline polymer is maintained at relatively low values up to the melting temperature and increases rapidly near the melting temperature. Above the melting temperature, the loss modulus again decreases rapidly [45]. The material used in this study, Nylon 6, is stiffer and more heat resistance compared to a pure polymer material owing to its reinforcement with short carbon fibers, which contributes to greater interfacial rather than intermolecular friction.

Annealing this material increases its stiffness, as expressed by the storage modulus, and its resistance, as expressed by the glass transition temperature. These increases lead to higher heat generation due to interfacial friction and improve the welding process at the same welding energy level compared with as-received samples.

3.4.4. Temperature Evolution and Maximum Temperature in USW

The maximum temperature during USW and the evolution of temperature were measured, and the evolution of temperature is shown in Figure 3.15(a). Figure 3.15(a) confirms that the temperature evolutions for the USW of the as-received and annealed coupons are different. Annealing at 180°C leads to the most rapid temperature increase and the highest maximum

temperature. The maximum temperatures during USW are shown for five replicates in Figure 3.15 (b).

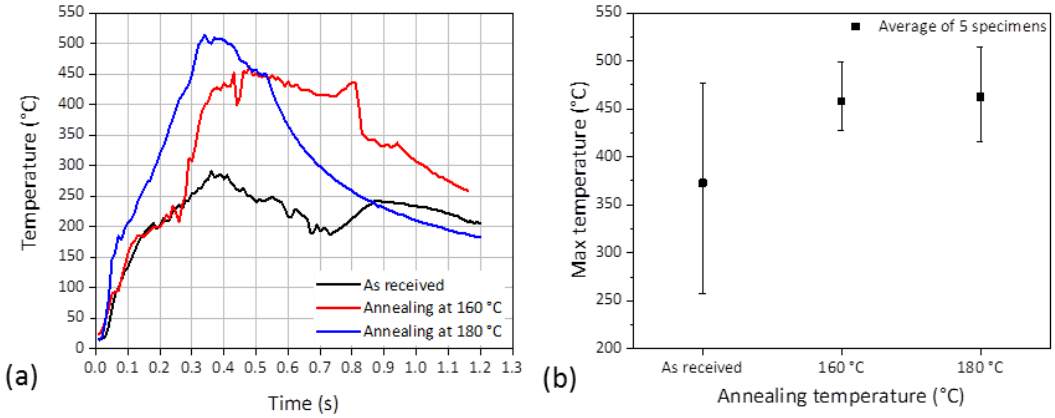

Figure 3.15 (a) Temperature evolution during USW of as-received and annealed CFRP, (b) Maximum temperature measured during USW of as-received and annealed CFRP

3.4.5. Mechanical Property

The material's ultimate tensile strength is shown in Figure 3.16, which illustrates the increase in ultimate tensile strength with increased annealing temperature. This phenomenon can be explained by the increase of the α crystalline form, which improves tensile strength, in the material after annealing. Higher tensile strength of base material influences the weld strength after USW.

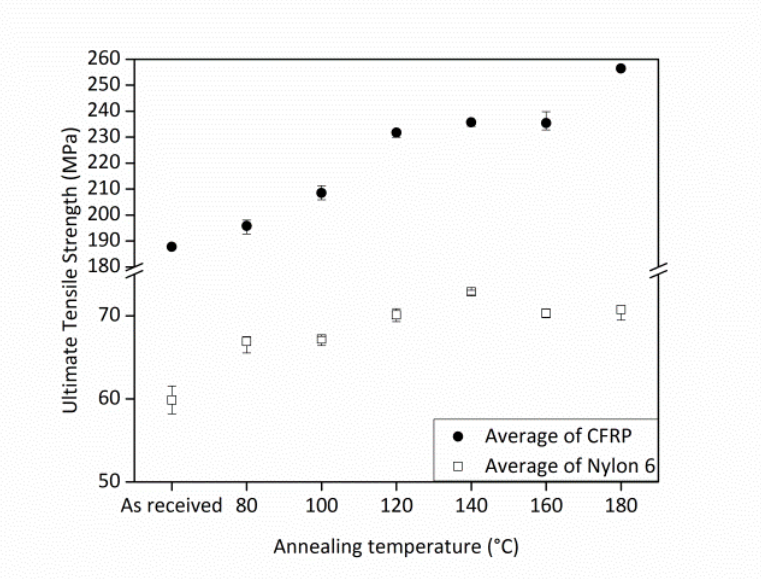

Figure 3.16 Mechanical property of CFRP and Nylon 6 as received and annealed

3.4.6. Weld Strength

The weld strengths by single lap shear test are shown in Figure 3.17. The maximum lap shear load increases with the increase of annealing temperature. These results prove the influence of the morphological parameters, viscoelastic and mechanical properties on USW. With annealing at 160 °C, various welding energy levels (600, 700, and 800 J) are used to validate the influence of morphological parameters, viscoelastic and mechanical properties on weld strength (Figure 3.18).

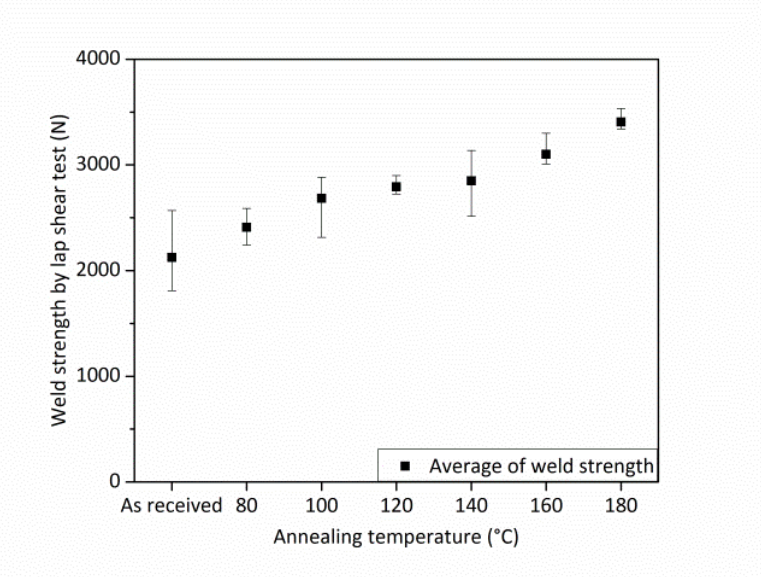

Figure 3.17 Weld strength of CFRP as received and annealed

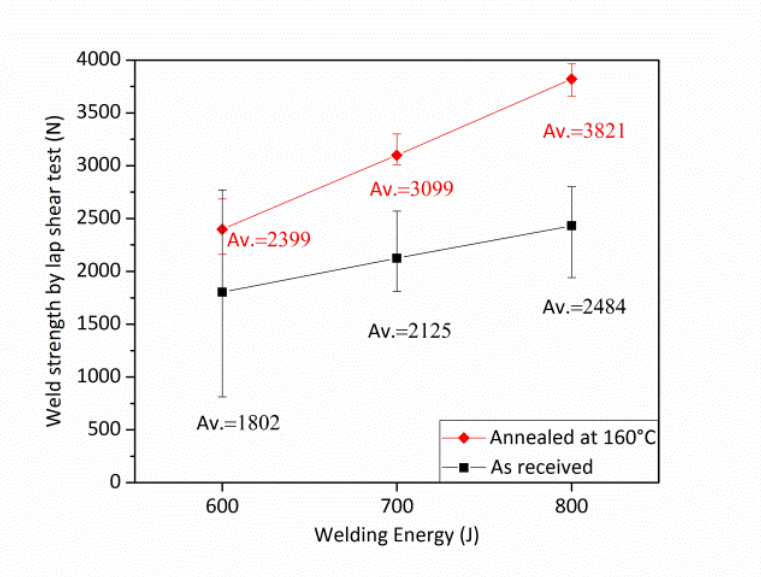

Figure 3.18 Weld strength of CFRP with various welding energies (600, 700, and 800 J) for the cases as received and annealed at 160°C (where Av. is the average of weld strength)

Figure 3.18 shows that not only did the average weld strength increase, but also that the variation in weld strength decreased. This result demonstrates that the better DoC distribution and higher weight fraction of the α crystalline form compared to the γ crystalline form change the

viscoelastic properties of the material. These parameters can be defined as morphological parameters that influence the material's viscoelastic and mechanical properties. These changes permit a more stable and efficient welding process. The weld strength is also improved through enhancement of the mechanical properties of the material itself. In this study, the average weld strength improved on average by 46% and variation in weld strength decreased on average by 61%.

3.5. Conclusions

In this research, morphological parameters are introduced, such as DoC and the weight fraction ratio of crystalline forms, in Nylon 6 to study the USW of short carbon fiber polymer composite materials without energy directors. Introducing an annealing process enables control of the morphological parameters and study of their influences on the material's viscoelastic and mechanical properties. Changes in viscoelastic and mechanical properties are demonstrated to alter heat generation during USW and the resulting weld strength. The conclusions of the study are as follows:

(1) Morphological parameters, such as the DoC and the α/γ ratio, influence the material viscoelastic and mechanical properties, which are important parameters for USW. Morphological parameters must be considered to control the USW performance.

(2) Annealing can be used to control the material's morphological parameters, inducing a uniform DoC distribution. The α/γ ratio increases with annealing temperature.

(3) The uniform DoC and increased α/γ ratio obtained by annealing increase the storage and loss moduli and the glass transition temperature of the material, which results in more efficient USW, in terms of heat generation by interfacial and intermolecular friction. These changes in the morphological parameters also cause the material to have a higher ultimate tensile strength.

(4) The improved viscoelastic and mechanical properties lead to higher average and less variable weld strengths.

Chapter 4 Process Modeling of Ultrasonic Welding of Carbon Fiber Reinforced Plastics without Energy Directors

In this chapter, a finite element model (FEM) is developed to simulate the heat generation and weld formation during ultrasonic welding of short carbon fiber polymer based composites. This model serves a robust tool for studying the influence of the process parameters, such as trigger force, welding time, welding speed, and horn amplitude on the welding attributes such as weld area. Other important applications of this model are the prediction of the heat generation and its propagation in the workpieces during welding and the calculation of the energy efficiency of the USW for different cases.

The novel characteristics of this model are: (1) an improved description of the heat generation taking into account the component generated by the friction, and (2) a new description of the material behavior under high frequency and temperature as used in USW. This model is validated through comparing the temperature profile obtained from the USW experiments and simulation.

In the following sections, details of the FEM model are presented for the USW of two workpieces made of short carbon fiber composite CFRP, namely HiFill PA6 CF30. The material characteristics of HiFill PA6 CF30 were presented in Chapter 3. Thus, Section 4.1 describes the model set-up; Section 4.2 discusses the simulation results and their validation; Section 4.3 summarizes the chapter with conclusions.

4.1. Model Configuration

In this section, a FEM model for USW process is developed to investigate the temperature, strain and displacement distribution during welding. The FEM model uses the experimental set-

up which can be found in Chapter 3. Several tests were conducted to generate the material properties used in the FEM.

4.1.1. The Finite Element Model - Geometry, Mesh, Boundary Conditions and Contact

Geometry: The model consists of four parts: a horn, a top workpiece, a bottom workpiece, and an anvil. The horn is made of steel and the anvil is made of aluminum. Figure 4.1(a) shows the geometry of the model which fully mimics the experimental conditions presented in Chapter 3.

(1) Anvil: The aluminum anvil is a support part that the workpieces are placed on. The anvil has two sections of different thicknesses to accommodate the bottom workpiece. The width of the anvil is 38 mm.

(2) Horn: The steel horn is the moving part in the ultrasonic welding process. The shape of the horn is a cylindrical solid with a constant cross section of 9.5 mm in diameter and 20 mm in length.

(3) Top and bottom specimens: The top specimen and the bottom specimen have a hexagonal shape and the same dimension (38mm x 127mm x 3mm). The shape and dimension come from the experimental setting. The specimens are made of CFRP. The length of overlap is 38mm.

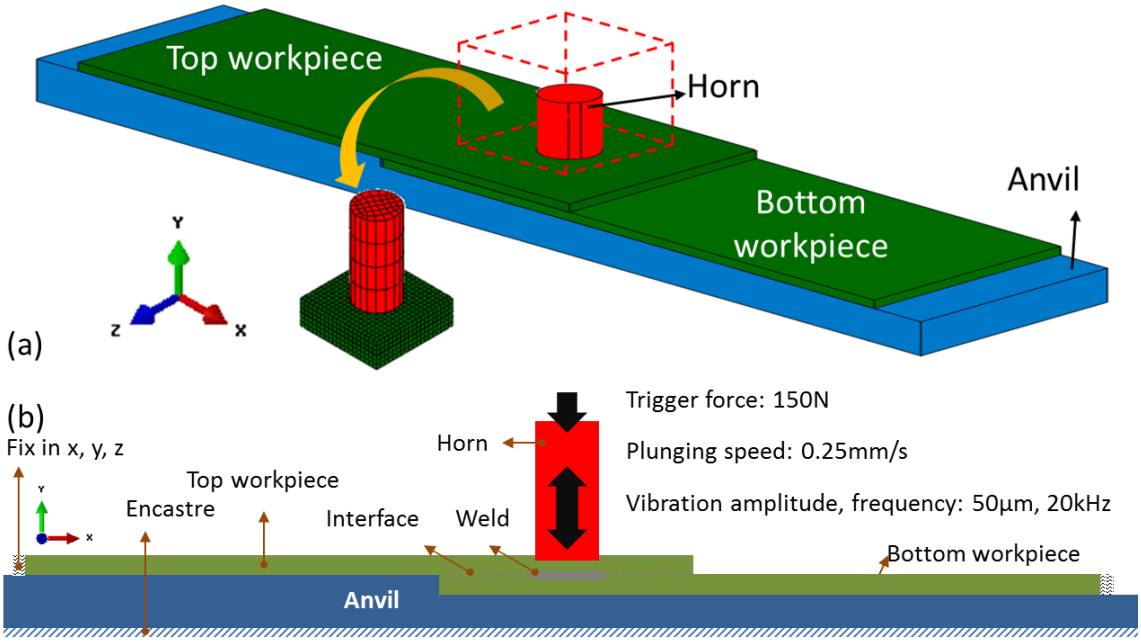

Figure 4.1 Description of the finite element model: (a) Geometry, (b) Scheme of parts and boundary condition

Abaqus v14.1 Explicit is used for this model to address the issues of divergence and the large computation costs due to the non-linearity of material property and high strain rate of vibration in USW process.

Mesh: A hybrid mesh involving two types of finite elements is used: a linear reduced integration hexagonal solid element C3D8RT, and a full integration solid element C3D8T. In general, the element types (C3D8RT and C3D8RT) allow thermo-mechanical coupled calculations which are needed for the USW process. Both elements are designed to calculate thermo-mechanical stress and strain states. For the sake of computation time of the simulation process, C3D8RT element was used for meshing the two workpieces except a limited volume of 1mm^3 situated under the horn. For this volume, C3D8T type element was used. Reduced integration scheme of C3D8RT provides enough accuracy of the results in the stress, strain and heat generation in the workpieces but for high fidelity results in the welding area (situated under the horn) a full

integration scheme is used. Thus, the hybrid mesh allows a good balance between the computation time of simulating USW (around 72h on 200 CPU cores) and the accuracy of the results especially in the weld area where complex thermo-mechanical phenomena are overlapped in time and space. The mesh size for the workpieces is 7.5 mm x 7.5 mm x 1 mm, for anvil is 5 mm x 5 mm x 5 mm and for the horn it is 5 mm x 1 mm x1 mm. Under the horn, the mesh size is 1 mm x 1 mm x 1 mm.

Boundary Conditions: The USW process was simulated in three steps and the boundary conditions evaluated in the experimental conditions were reproduced in the simulation. The three steps are: (1) the initial step of mechanical clamping, (2) the trigger step of vibration initiation, and (3) the vibration step of the full application of the vibration. An illustration of the three steps is presented in Figure 4.2.

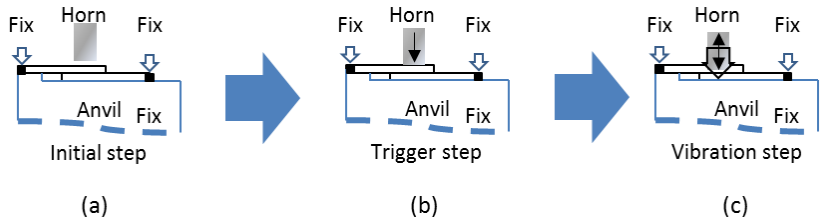

Figure 4.2 Decomposition of the USW process in three steps: (a) Initial step, (b) Trigger step and (c) Vibration step

In the initial step (Figure 4.2.(a)), the mechanical clamping is ensured through the following boundary conditions: (1) the bottom surface of anvil is fixed in all degrees of freedom, and (2) the lateral edges of the workpieces are limited in their movement in the Y-direction. These conditions are necessary because even the vibrations are applied through the horn in the Y direction, they propagate also in the X-Z plane producing relative movement of the two workpieces and leading

to dissipation of the energy in locations which are not belonging to the weld area. That is why, experimentally, these movements are blocked using a dedicated anvil.

In the same step, the initial temperature is set-up to 20°C for all the parts. Heat transfer is allowed only through the interfaces: horn-top workpiece, the two workpieces and workpiece-anvil. It is assumed that there is no heat transfer between the four parts and the air.

These conditions are mapped into the next two steps which are the trigger step and the vibration step (Figure 4.2(b) and Figure 4.2(c)). The welding parameters as used in the experiments are imposed in these steps. There are five welding parameters used in this model: (1) the welding energy defined as the mechanical energy that is provided to the system during welding - W(J); (2) the welding speed defined as the linear speed at which the horn moves downwards during the process - v(mm/sec), (3) the amplitude defined as the magnitude of vibration of the ultrasonic horn during the process - A(μm), (4) the welding frequency defined as the frequency of ultrasonic vibrations - ω(Hz), and (5) the trigger force that the horn exerts on the overlapped samples before the vibration begins - F(N).

In the trigger step, an initial displacement of the horn is applied to simulate the trigger force which clamps the two workpieces by a compressive pressure. This contact pressure determines a full contact between the two workpieces by flattening the surfaces. This step starts simultaneously with the vibrations. Thus, the flattening of the surfaces in contact will be done through a relative motion between the two workpieces which consequently generates the heat. Further, the movement of the horn has a combined trajectory which can be described as a composition of two phases:

- phase 1 (0 s - 0.16 s): a linear displacement and a sinusoidal displacement in Y direction with a continuously increased amplitude up to a maximum value which is set-up at the beginning of the process (e.g. A= 50μm) and

- phase 2 (0.16 s - 1 s): a linear displacement and a sinusoidal displacement in Y direction with a constant maximum amplitude.

Contact: The contact between the two workpieces is defined as the "surface-to-surface" contact in Abaqus [73] with two components: (i) normal to the surface of the workpiece where separation is allowed during vibrations, and (ii) tangential to the surface of the workpiece where a penalty friction model is used combined with a temperature-dependent friction coefficient.

Because USW involved thermo-mechanical phenomena where the friction dissipation energy will be transformed into heat energy, a "conductance thermal contact" [73] is defined at the interface between the two workpieces. The thermal contact of the other interfaces: horn-top workpiece and bottom workpiece-anvil was defined as a "general contact" [73] using the friction coefficients corresponding to metal-polymer contact. The values of these friction coefficients were chosen from literature [68].

4.1.2. Constitutive Material Model

The material used for the workpieces is HiFill PA6 CF30. This material is a CFRP with 30 % weight fraction of short carbon fibers and a Nylon 6 matrix. The density of CFRP is 1.272 g/cm^3. The coefficient of thermal expansion is 21 x 10^{-6} /°C. The thermal conductivity is calculated using Halpin-Tsai equation (Equation 4.1) [69] which gives a value of 2.018 W/m/K.

$$k_{CFRP} = \frac{1}{\rho_{CFRP}} (V_f \rho_f k_f + V_m \rho_m k_m) \qquad \text{(Eq. 4.1)}$$

where k_{CFRP}, k_f, k_m are thermal conductivity of CFRP, carbon fiber, Nylon 6 respectively. ρ_f, ρ_m are density of carbon fiber and Nylon 6 respectively. V_f, V_m are volume fraction of carbon fiber and Nylon 6 respectively.

Heat Capacity: The heat capacity is measured using DSC analysis. In this analysis, samples of 10mg were collected from a CFRP workpiece and heated from the room temperature (20°C) up to 270°C with a heating and cooling rate of 10°C/min. The heat capacity is determined by the following equation (Equation 4.2).

$$C_p = \frac{1}{m} \times \frac{dQ/dt}{dT/dt} \qquad \text{(Eq. 4.2)}$$

where C_p is the heat capacity of specimen, m is the mass of specimen, $\delta Q/dt$ is the heat flux given by DSC, and dT/dt is the heating rate of the specimen.

Heat capacity at values greater than 270°C are needed because in USW the maximum temperature during welding could reach 450°C [10]. Because of the existing DSC equipment is limited to heating up to 270°C, the heat capacity from 270°C to 600°C is calculated by applying the rule of mixtures to the values corresponding to the short carbon fibers and for the Nylon 6 matrix found in the literature [70-72]. By combining the measured and the calculated values, a full profile of the heat capacity of the HiFill PA6 CF30 is obtained (Figure 4.3).

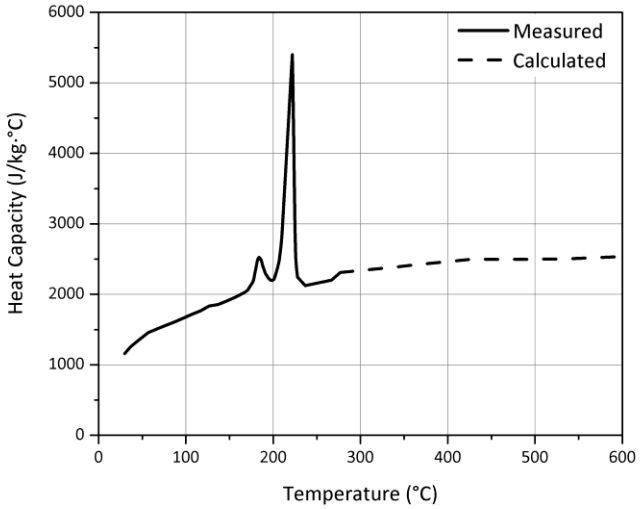

Figure 4.3 Heat capacity of CFRP: Measured using DSC for the range 0°C to 270°C and calculated for the range 270°C-600°C

Friction Model: Temperature-dependent friction coefficients were measured within an experiment set-up. The configuration of this test is similar to a lap shear in which the samples have an overlap of 38mm (Figure 3.8, Chapter 3). In this experiment, three slip rates (0.1 mm/min, 5 mm/min and 250 mm/min) were used to measure the friction between the two workpieces. The friction coefficients measured from experiments with varying temperatures and slip rates are shown in Figure 4.4.

During USW experiments, it was noticed that the slip rate at the interface between the two workpieces varies depending on the welding time and the distance from the center of horn and to the edge as shown in Figure 4.5. At the location under the center of horn, the displacement in the horizontal direction is zero. The displacement becomes larger according to a radial direction of the horn at the interface of the workpieces due to the compression load of horn. From the difference of displacement at the interface, the slip rate is also varied as the displacement changes. As the welding time varies, the displacement become larger because the horn is moving downward during

the USW process. Consequently, the friction coefficient variation due to the liner displacement of the horn was plotted with the distance from the center of the horn toward the edges of the workpieces for the slip rates between 0 mm/min - 250 mm/min (Figure 4.5). The slip rate (40,400 mm/min) due to the vibration of 20 kHz in USW process could not be measured. Physical determination of the friction coefficients for this slip rate is impossible due to experimental limitations. Hence the friction coefficient variation corresponding to the highest slip rate used in the experiments (up to 250 mm/min) is used in the model.

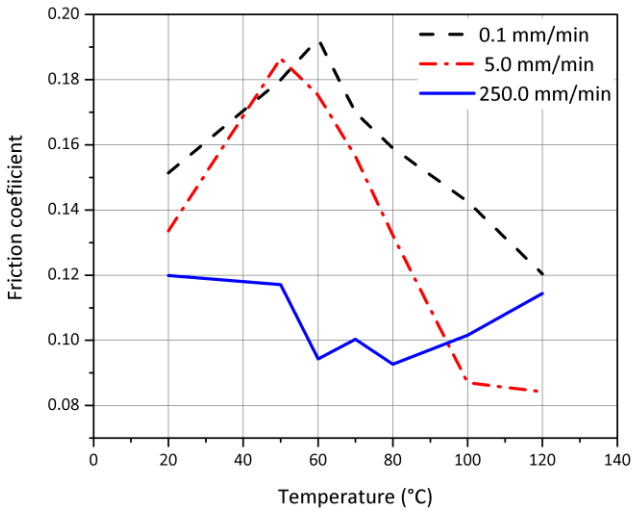

Figure 4.4 Evolution of the friction coefficient of CFRP with the temperature. Three slip rates were used for a variation of temperature from 20°C to 120°C.

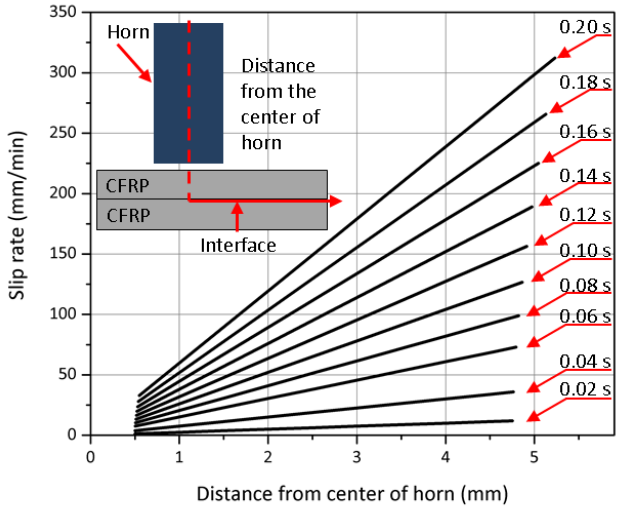

Figure 4.5 The gradient of the slip rate at the interface of workpieces from the center of the horn toward the edges. Welding time is between 0.02 second and 0.2 second.

Viscoelastic Properties: DMA analysis was applied for temperatures between 0°C ~ 350°C and frequency between 1 Hz ~ 100 Hz with 0.1 % of strain amplitude. This maximum frequency of 100 Hz is a limitation of the existing versions of the DMA equipment. To characterize the material at a higher frequency, e.g., 20 kHz corresponding to the USW process, the time-temperature superposition methods with the Williams-Landel-Ferry (WLF) equation was used to obtain the shift factors.

For polymers and polymer composites, the elastic modulus (E^*) has a complex form (Equation 4.3) with a real part which is the storage modulus (E') and an imaginary part which is the loss modulus (E'').

$$[E^*] = \sqrt{E'^2 + E''^2} \qquad \text{(Eq. 4.3)}$$

This form in used in the finite element simulation. Abaqus uses the Prony series as one of the versions of describing this behavior. Thus, the Prony series (Equation 4.4) are calculated using the DMA results and input in the material model.

$$\varpi\Re(g^*) = G_L/G_\infty, \quad \varpi\mathrm{I}(g^*) = 1 - G_S/G_\infty \qquad \text{(Eq. 4.4)}$$

where $\omega R(g^*)$ and $\omega I(g^*)$ are real and imaginary part of a Fourier transformation of non-dimensional shear relaxation function, , G_S and G_L are storage and loss modulus, G_∞ is long-term shear modulus determined from the elastic property.

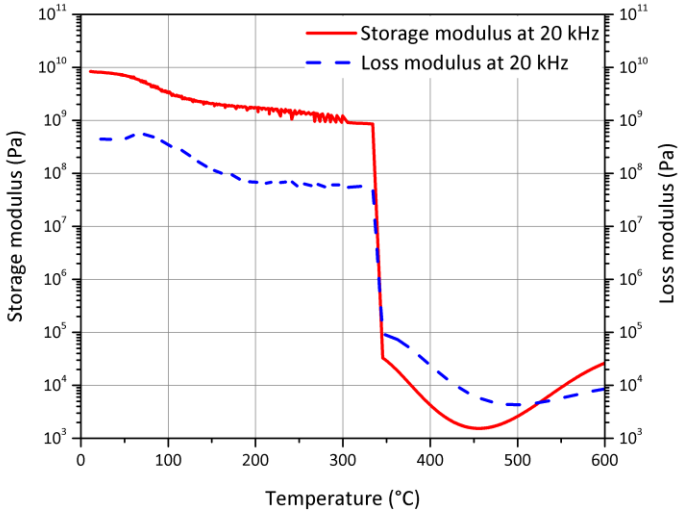

Figure 4.6 Viscoelastic properties of CFRP measured determined using the DMA analysis and shifted by using time-temperature superposition method (solid red: storage modulus, dash blue: loss modulus at 20 kHz)

The FEM model for CFRP demands the temperature dependent characterization of the materials in elastic and viscoelastic behavior. In terms of elastic behavior, Young's modulus and Poisson's ratio are defined with temperature change from room temperature to melting

temperature. The FEM model does not take into account the phase change between solid and liquid but the Young's modulus above the melting temperature is defined with the combination of storage modulus and loss modulus from viscoelastic properties. The elastic modulus above melting temperature is quite low so that liquid phase is expressed in terms of elastic modulus.

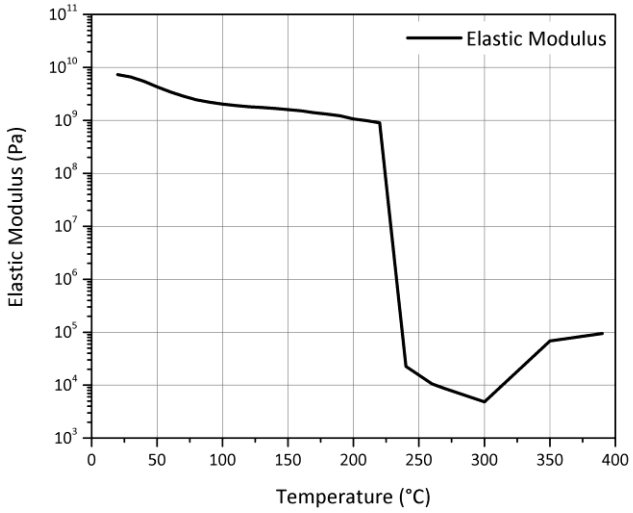

Figure 4.7 Elastic modulus of CFRP in terms of bulk modulus measured by DMA at 1 Hz with 0.002 /s of strain rate

4.1.3. Particularities of the Equilibrium Equation for the Finite Element Method

The governing equation in the present finite element model is determined by the conductive heat transfer. The heat generated at the interface between the two workpieces (Q) is composed of an interfacial friction heating component and an intermolecular friction heating component. The governing equation (Equation 4.5) is shown as below.

$$k\frac{\partial^2 T}{\partial x^2}+k\frac{\partial^2 T}{\partial y^2}+k\frac{\partial^2 T}{\partial z^2}+Q-\rho c\frac{\partial T}{\partial t}=0 \qquad \text{(Eq. 4.5)}$$

where k is thermal conductivity, Q is volumetric heat generation rate, ρ is density, c is specific heat capacity.

The interfacial friction heating component of the heat generation is dominant at the beginning of the process when the vibration is applied and as the intermolecular friction heating component becomes dominant as the strain and temperature of workpieces increase [30]. The interfacial friction heating component of the heat generation is dominant at the beginning during the process when the oscillation of horn is subjected to cyclic displacement and the intermolecular friction heating component becomes dominant as the strain and temperature of workpieces increase. The average dissipated energy rate [$J/s \cdot m^2$] by friction at the interface of the parts during USW process can be expressed with the below equation.

$$\dot{q}_{interfacial} = \alpha^2 \frac{\varpi}{2\pi} \int_0^{2\pi/\varpi} \mu \left|\sigma_{yy}(x,z)\sin(\varpi t)\right| \cdot \left|\frac{d\delta u(x,z)\sin(\varpi t)}{dt}\right| dt = \alpha^2 \frac{\varpi \mu}{\pi} \left|\sigma_{yy}(x,z)\,\delta u(x,z)\right|$$

(Eq. 4.6)

where α is hammering effect coefficient, ω is vibration frequency, μ is the friction coefficient, σ_{yy} is the vertical stress on the horizontal interface, δu is the horizontal displacement discontinuity across the interface.

The average dissipated strain energy per volume by viscoelastic damping [$J/s \cdot m^3$] subjected to a sinusoidal strain ($\varepsilon = \varepsilon_0 \sin(\omega t)$) is directly used in this heating mechanism as below equations.

$$\sigma\dot{\varepsilon} = (E'\varepsilon_0 \sin(\varpi t) + E''\varepsilon_0 \sin(\varpi t))(\varepsilon_0 \varpi \cos(\varpi t)) \qquad \text{(Eq. 4.7)}$$

$$\dot{q}_{intermolecular} = \alpha^2 \frac{W}{2\pi/\varpi} = \alpha^2 \frac{\int \sigma \dot{\varepsilon} dt}{2\pi/\varpi} = \alpha^2 \frac{\pi E'' \varepsilon_0^2}{2\pi/\varpi} = \alpha^2 \frac{\varpi E'' \varepsilon_0^2}{2} \quad \text{(Eq. 4.8)}$$

where α is hammering effect coefficient, σ is stress, W is total work done per cycle, ε is the strain, ε_0 is an amplitude of strain, E' is storage modulus and E'' is loss modulus.

Finally, the summation of the interfacial friction heating and intermolecular friction heating in CFRP parts will be used as a heat source (Q) of Equation 4.5.

4.2. Results and Discussion

Validation of the model is carried out through comparing the predicted heat generation, temperature and the welding area with the experimental results. The following paragraphs provide details of this validation process.

4.2.1. Prediction of the Heat Generation

As mentioned in the previous paragraph, heat generation in the USW process is assumed to be a combination of an interfacial friction heating and an intermolecular friction heating. To understand the role of each component during the USW process, the model was used to simulate the heat generation considering either only interfacial friction heating or only intermolecular friction heating.

For the case with only interfacial friction heating, the prediction of the heating evolution is presented in Figure 4.8. Because this case is dominated by the friction, the simulations were done with different friction coefficients corresponding to the three slip rates used in 4.1.2. As shown in Figure 4.8, the heating curves have a significant increase from the beginning of the welding process at the area under the edges of the horn and almost no increase in the center of the weld under the horn. This conclusion supports the fact that the interfacial friction heating has an important role in

initiation of the heat generation. However, the weld formation doesn't start from the center of the horn.

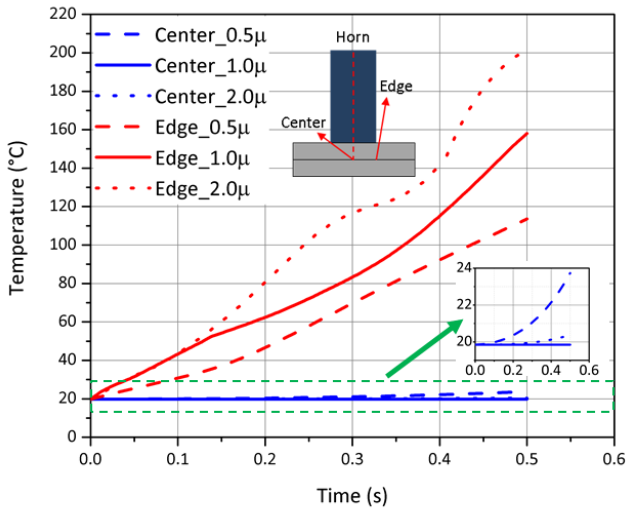

Figure 4.8 Temperature at the interface: The area under the center of horn and the area under the edge of horn only with interfacial friction heating, friction coefficients corresponding to 0.5, 1.0, and 2.0 times of friction coefficients of CFRP.

A second case was simulated where the heating is generated only by the intermolecular friction heating. The heat generation curves are presented in Figure 4.9. The curves show that the intermolecular friction heating is not generated at the beginning of the process but after glass transition temperature is reached in the matric (T_g=60°C). This conclusion is perfectly consistent with the literature indicating that an intermolecular friction mechanism is activated when the polymer reaches T_g.

Analyzing the welding time when the two mechanisms are changing their roles, it can be concluded that in the first 0.2-0.4s of the USW process, the heating is generated by interfacial friction and it is localized toward the edges, far from the center of the weld. After 0.4s, the

intermolecular friction heating starts to be dominant and the heating is accelerated. Thus, the center of the weld will start to be melted and generate the weld, so called nugget in welding community.

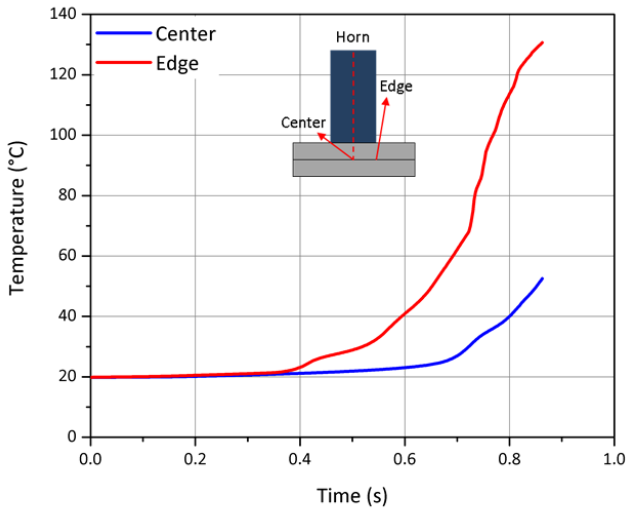

Figure 4.9 Temperature at the interface: the area under the center of the horn and the area under the edge of the horn only with intermolecular friction heating source

These two heating sources are combined in USW process and the physical phenomena by the heating are shown in FEM model. Figure 4.10 shows the horizontal displacements in X-Z plane and Figure 4.11 shows the vertical stress at the interface between two workpieces where the weld forms. The horizontal displacement of the workpiece at the interface is much larger than the area under the horn. The vertical stress is much higher for the area under the center of the horn but the horizontal displacement is almost zero because the horn prevents the movement of workpieces through a mechanical clamp. As a result, the heat generation starts from the area corresponding to the edge of the horn toward its center. After 0.2s, Figure 4.11 shows that the vertical stress at the edge of the horn area becomes almost zero which means the interfacial friction heating becomes smaller due to the fact that the matrix of the composite is starting to be melted.

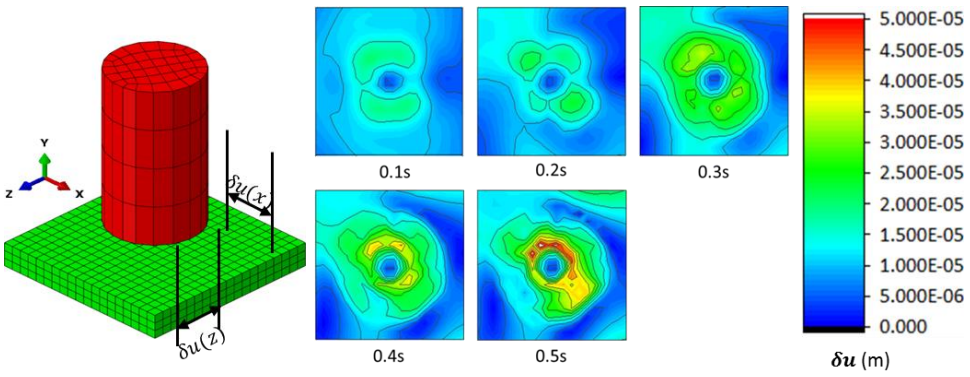

Figure 4.10 Horizontal displacement contours in X-Z plane at the interface

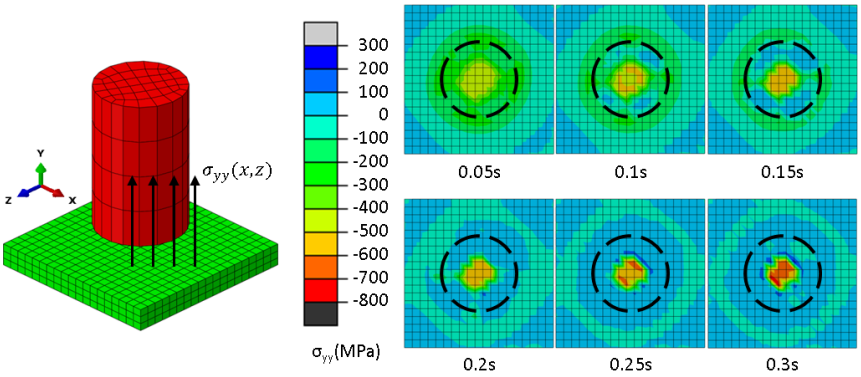

Figure 4.11 Vertical stress contours at the interface

This conclusion could be confirmed by the experimental investigation of USW applied to a HiFill PA6 CF30 workpiece and a Nylon 6 one. A Nylon 6 workpiece was used with the purpose of visualization of the welding line which is not possible to be seen in the welding of two HiFill PA6 CF30 workpieces. The cross section of a USW weld is presented in Figure 4.12. The observations were done in three areas of the welding zone, one corresponding to the area under the center of the weld, under the horn (b) and two situated at the edge of the horn (a and c).

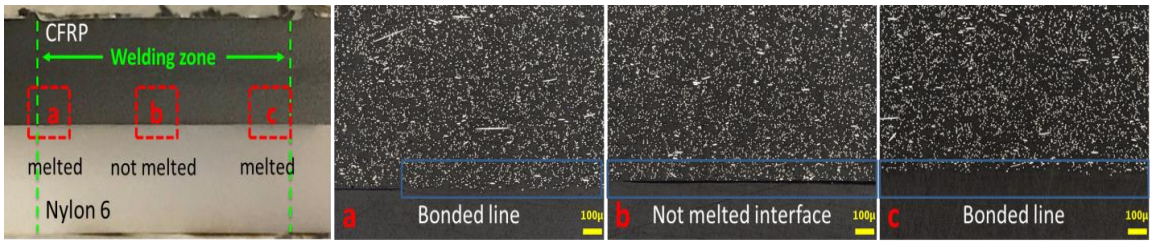

Figure 4.12 Cross section of the USW weld zone along the workpieces

As shown in the three magnified images in Figure 4.12, the two surfaces are bonded in the Figure 4.12 (a) and Figure 4.12(c) cases and unbonded in the case of Figure 4.12(b). This observation is in a good agreement with the model prediction of the weld formation.

4.2.2. Prediction of the Temperature Evolution at the Interface

The temperature evolution is the most important information in the USW process as it is related to the heat generation. However, physical measurements are challenging due to the enclosure of the welding area and short welding time. Following an extensive program of trials, an optimized set-up of recoding the temperature evolution was done. For measuring the temperature, the various process parameters such as welding energy were used. The Arduino temperature measurement system (Figure 4.13) can generate the temperature information every 0.01 second.

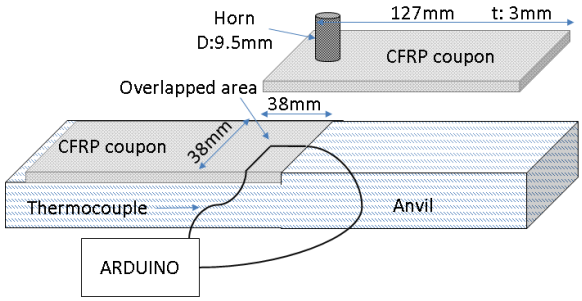

Figure 4.13 Experimental set-up of temperature measurement during the USW process

The experimental results were compared with the simulation results. From the thermocouple and the Arduino system, the highest temperature is recorded every 0.1 second among the temperatures which can be measured on the interface of two workpieces. Thus, the profile of the temperature over time will be plotted. One example of the prediction of the temperature is presented in Figure 4.14. As shown in the figure, there is a very good agreement between the predicted and the measured although there is a slightly overestimation of the highest temperature (e.g. 250°C instead of 220°C) for welding energies between 600-800J. After melting starts at 220°C for Nylon 6 matrix, the heat generation propagates from the edges of the horn toward the center. Melting of the volume of the material under the horn though surrounded by a melted ring will create an adiabatic reaction leading to a constant temperature. The temperature will remain constant until all the volume under the horn is melted. Right after this moment, the temperature increases slowly until above 300°C followed by an accelerated increase due to large strains produced in the viscous material.

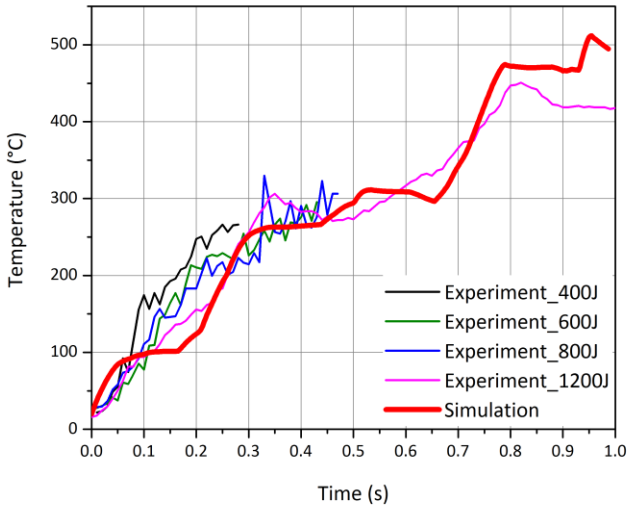

Figure 4.14 Comparison of the predicted and measured maximum temperature during USW process of CFRP

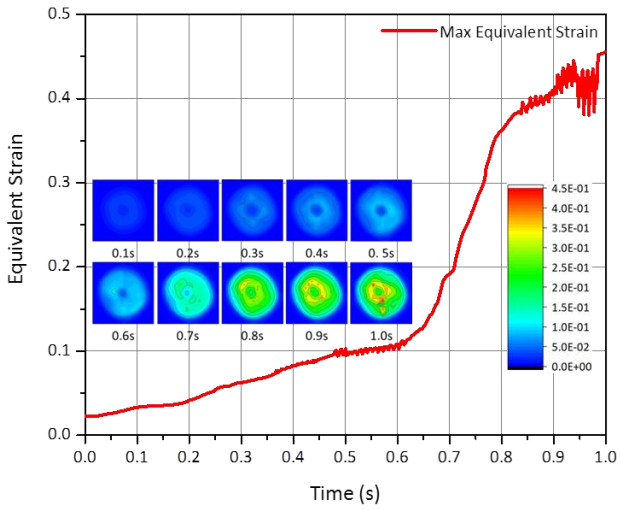

Figure 4.15 Evolution of the equivalent strain contour under the horn and the equivalent strain evolution

Figure 4.15 shows a linear increase of the equivalent strain absolute value until 0.6s followed by a non-linear increase after 0.6 s. This evolution perfectly explains the weld formation steps: up to 0.6 s, the friction dissipation energy is transformed in heat and the heat will start to trigger the

viscoelastic behavior. Once 0.6 s is reached, the heat generated leads to a temperature corresponding to melting of the composite matrix where the strain exponentially increases due to the loss of the stiffness of the matrix. USW is also classified as a warm forming process due to the fact that the composite will deform first followed by melting. That is why the equivalent strain is analyzed depending on the welding time.

4.2.3. Prediction of the Weld Formation

The weld area is one of the welding attributes influencing the weld strength. The weld size is proportional to the weld strength for a good quality weld [10] and is mostly determined by the heat generation during USW process. Prediction of the weld area is an effective approach in validating the model. Weld formation is a progressive process where different final elements will reach the melting temperature and become part of the weld nugget. An algorithm for calculating the weld area was designed. Thus, the weld area for a given welding time is calculated by summation of the area of elements which have a temperature higher than the melting temperature (220°C). The values calculated by using this algorithm are compared with the experimental values. In the experiments, the weld area is measured after lap shear test. In Figure 4.16, comparison of the weld area at different welding times shows a good agreement between the simulation and the experiments.

As it can be observed, the weld starts to form at the edges of the horn and propagates toward the center of the horn. The qualitative and quantitative comparison shows a good agreement between the predicted values and the experimental ones. Figure 4.17 shows the weld growth according to the welding time for two different welding speeds (0.1, 0.25 mm/s). There are some variations in weld area in experiments but the trend of weld growth fits well with the FEM results.

From the simulation results, the weld size increases up to a certain welding time but the weld size saturates around 140 mm^2 which is twice the size of the horn surface area.

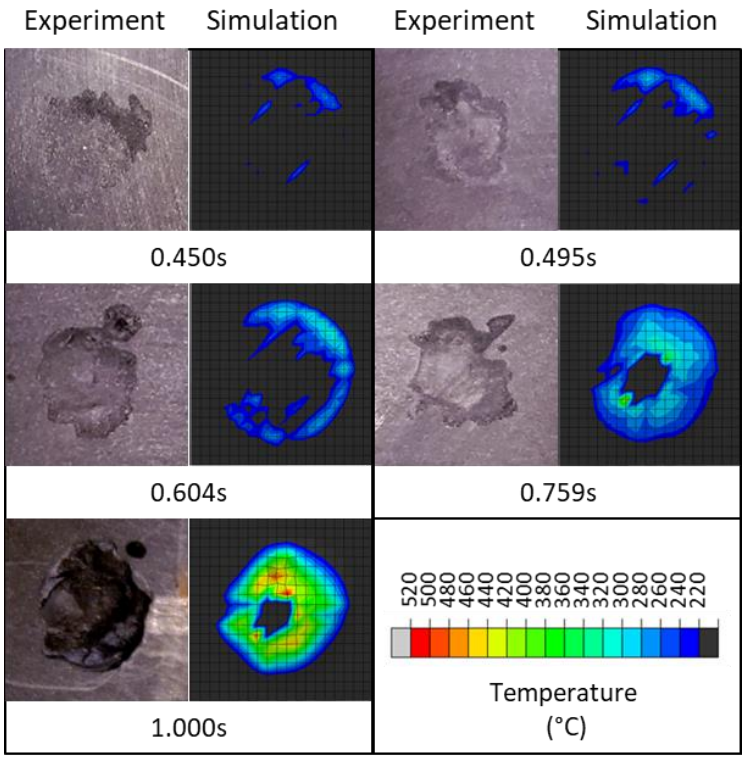

Figure 4.16 Weld evolution according to the welding time in experiments and FEM model with 0.25 mm/s of weld speed

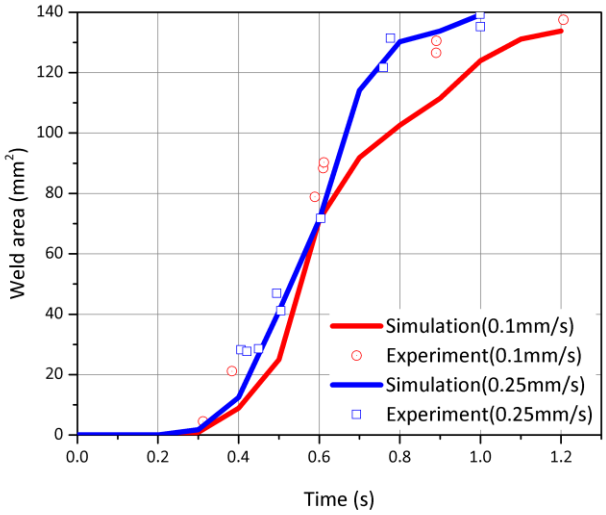

Figure 4.17 Comparison of the weld area formation for two welding speeds (0.1 mm/s and 0.25 mm/s)

4.2.4. Effect of Morphological Parameters on USW Process in FEM Model

From Chapter 3, it has been revealed that the morphological parameters change the viscoelastic properties of CFRP which are the most influential parameters in the intermolecular frictional heat generation in the ultrasonic welding process for CFRP. In this section, a FEM model with different viscoelastic properties has been built based upon different annealing conditions to confirm the results of Chapter 3.

The viscoelastic properties before annealing are measured to compare the heat generation depending on morphological parameters. The viscoelastic properties and simulation results in the previous sections in Chapter 4 are based on CFRP after annealing at 180°C. As received CFRP, which is before annealing, has lower viscoelastic properties than the case after annealing at 180°C as shown in Figure 4.18. The master curves of the storage modulus and the loss modulus at 20 kHz of frequency show that the viscoelastic properties after annealing at 180°C are higher than those of the as received CFRP from room temperature up to the melting temperature of CFRP.

The FEM model for ultrasonic welding process of CFRP as received workpieces shows that the lower temperature evolution and the lower weld area evolution compared with the previous results of CFRP after annealing at 180°C (Figure 4.19, Figure 4.20). And the simulation results are also validated with the experimental results by comparing the maximum temperature evolution during the ultrasonic welding process (Figure 4.21). These results confirm that the morphological parameters change the viscoelastic properties of CFRP and the changed viscoelastic properties influence the heat generation during the ultrasonic welding process for CFRP. The results correspond with the experimental results in Chapter 3.

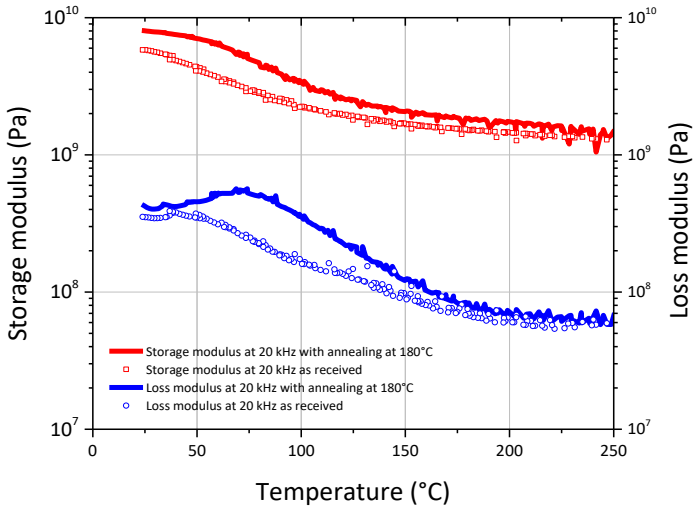

Figure 4.18 Comparison of the storage modulus and loss modulus of CFRP as received and with annealing at 180°C

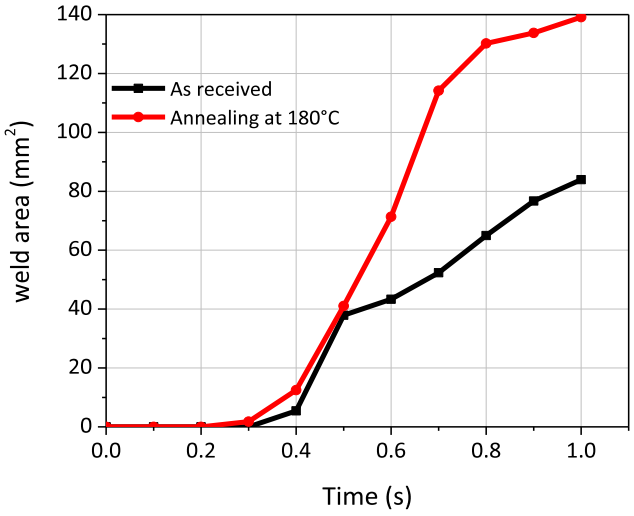

Figure 4.19 Comparison of the weld area evolution during ultrasonic welding of CFRP as received and with annealing at 180°C in simulation

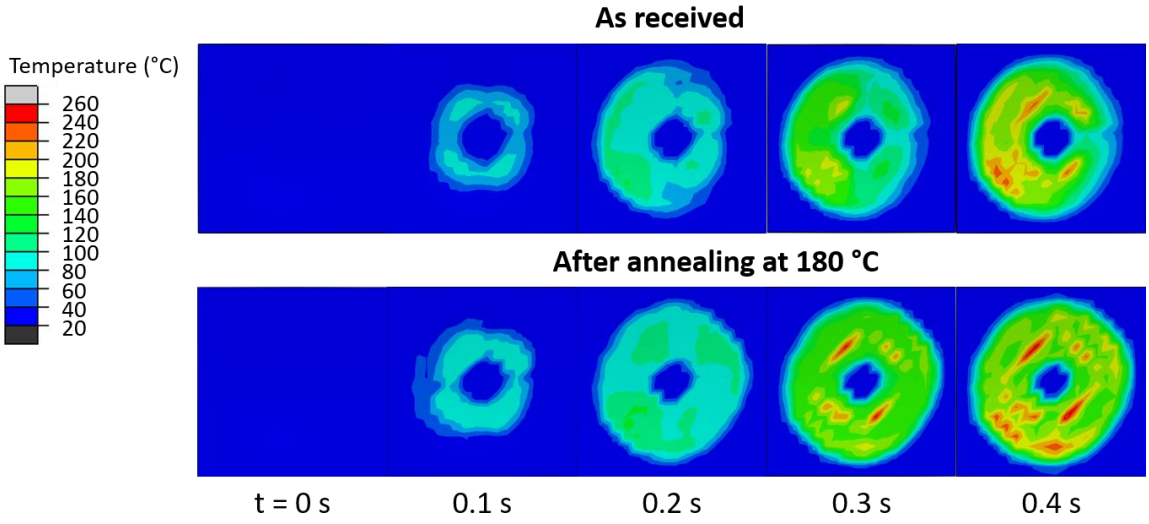

Figure 4.20 Evolution of temperature at the interface between workpieces during ultrasonic welding of CFRP as received and with annealing at 180°C in simulation

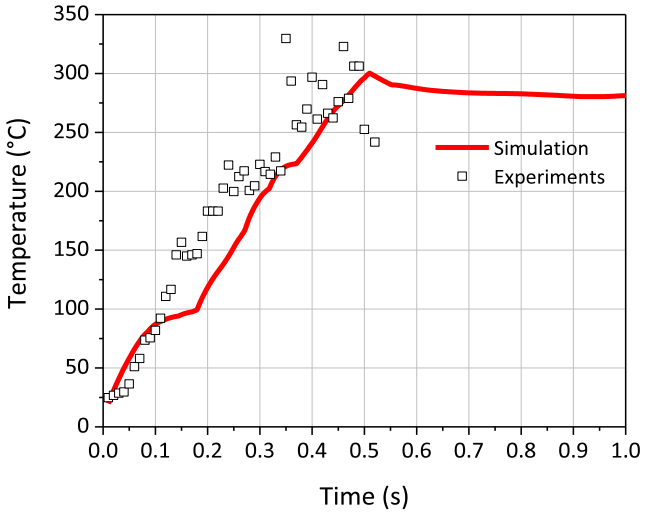

Figure 4.21 Comparison of the maximum temperature evolution during ultrasonic welding of CFRP as received in simulation and experiment

4.3. Conclusion

A FEM model was created to simulate the heat generation and weld formation in a USW process for CFRP without an energy director. This model was validated with the experimental results, demonstrating its accuracy in predicting welding temperature and weld area. The model provides a means for understanding the weld formation, which can lead to optimization of the process in order to reduce the variability of the welding strength, a challenge that is recognized by the welding community.

Using the developed model under certain process parameters, the following conclusions can be drawn:

(1) Interfacial friction heating is dominant at the beginning of the USW process (about 0.2-0.4s).

(2) Intermolecular friction heating becomes dominant after the glass transition temperature is reached in the matrix (after 0.4s).

(3) Heat generation rate produced by interfacial friction heating is dominant in the proximity of the edges of the horn and the heat generation rate produced by intermolecular friction heating is dominant under the center of horn.

(4) The heat generation rate is higher in areas closer to the edges of the horn due to both two heating mechanisms. As such, the areas under the edge of the horn began melting ahead of other areas.

(5) The weld forms at the edge first and propagates towards the center.

Understanding heating phenomena enables us to predict the weld area growth which contributes to weld performance. These are insightful conclusions which explain the weld formation in “CFRP”

Chapter 5 Dynamic Analysis of Ultrasonic Welding of CFRP according to Boundary Conditions

In this chapter, a finite element model (FEM) is developed to simulate the dynamic response of ultrasonic welding of short carbon fiber polymer based composites. This chapter is motivated by many experimental tests using USW for joining complex parts made of CFRP in the automotive industry. The experimental results have shown significant variations in the weld quality of CFRP depending on locations and sequences of the welding in a multiple spot configuration. The weld quality variation can be caused by surface variations of the parts caused by previous operations such as an injection molding, and positions of the welding spot with respect to the edges of the parts. These factors can change the vibration characteristics of the welding system. Vibration of the horn is the driving mechanism of ultrasonic welding process being strongly correlated with the wave propagation through the parts to be joined. Thus, the wave propagation can interfere with different edges of the parts, depending on its location. However, there are limited reports on investigating the effect of boundary conditions on the wave propagation in ultrasonic welding processes. For ultrasonic welding of metals, there have been several studies to analyze the effect of the dynamic response of ultrasonic welding system on the welding performance [47-50]. However, there has been few research for ultrasonic welding of polymers in spite of the importance.

For example, Yang et al. studied the strain change using Kevin-Voight model during ultrasonic welding with a blank holder representing a change in the boundary conditions of coupons to be joined [52]. The conclusion is that the blank holder has a constraint effect on the

welded parts leading to a concentration of the heat generation under the horn. The same study shows that an extended constraint applied to the parts lead to a low quality weld due to limitations in the relative displacement of the parts and, consequently, interfacial friction.

Therefore, to apply this knowledge from one welding spot to multiple spots of joining a complex part, an in-depth analysis of the interaction between the vibration propagation in a welding system and the weld quality of each spot is needed to further support design of the welding spots [74] as shown in Figure 5.1.

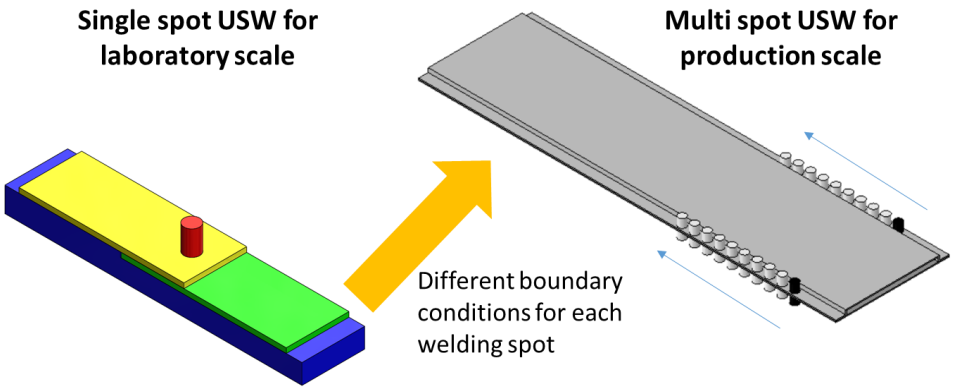

Figure 5.1 Difference of single spot USW and multi spot USW

Design parameters of the multiple welding spots are: (1) distance between the welding spots, (2) weld spot position with respect to the edges of the parts, and (3) horn size. To study the impact of these parameters on the weld quality, a welding system is considered to be composed of a U-shaped CFRP part joined with a flat CFRP part. Twenty weld spots symmetrically distributed on the U-shaped flange (10 on each side, 10mm distance between the weld central axes). The welding spots are numbered 1^{st} to 10^{th} in an ascending order from left to right. The configuration is presented in Figure 5.2. Boundary conditions between the two parts are changing as the welding moves from the 1^{st} spot toward the 10^{th} spot.

In the following sections, the influence of these boundary conditions on the welding growth is analyzed through the investigation of the dynamic response of the parts under vibrations produced by the horn. This study will be conducted for ultrasonic welding of two complex parts of CFRP as presented in Figure 5.2.

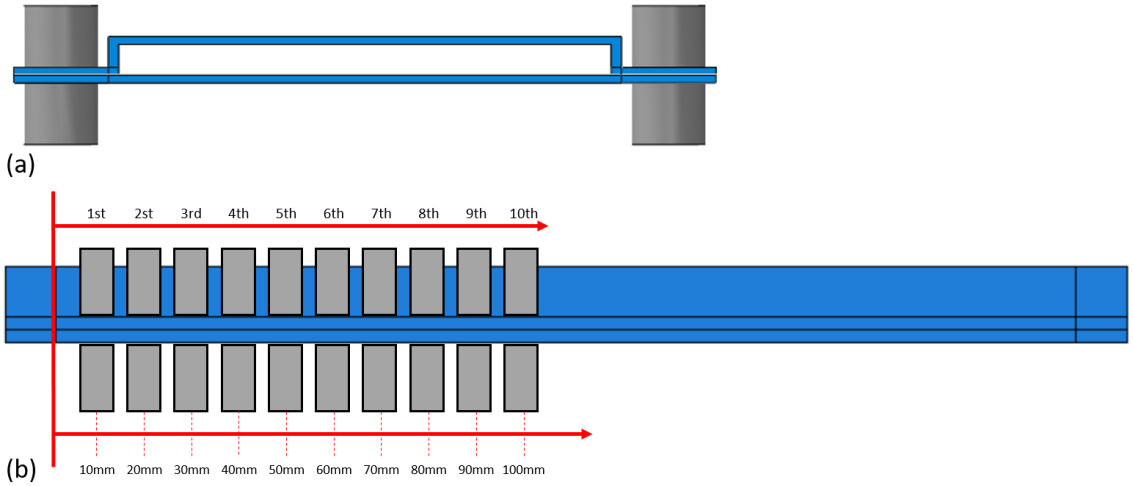

Figure 5.2 Selected joining configuration for dynamic response analysis: (a) Lateral view, (b) Front view. A U-shaped CFRP part will be joined to a flat CFRP part by 10 welding spots on each side. The initial welding design includes a 10mm distance between the welding spots, ordered from 1 to 10 starting from the one end of the parts. The horn diameter is 18mm. The flange of the U-shaped part has 23 mm.

Figure 5.3 is a flow chart showing an algorithm to investigate the relation between natural frequency and the welding performance. Dynamic FEM models for 10 welding spots are used to calculate the natural frequency of ultrasonic welding system and the maximum displacement at the natural frequencies. Relative displacement is defined as the ratio of the displacement at the frequency of 20k Hz which is the ultrasonic welding vibration frequency and the maximum displacement in the entire range of the calculation. Process FEM models for 10 welding spots are used to calculate the evolution of the heat generation and the weld area. Tendencies of changes in

the heat generation, the weld area and the relative displacement index are compared for 10 welding spots to confirm a hypothesis that the dynamic response of USW influence the welding performance.

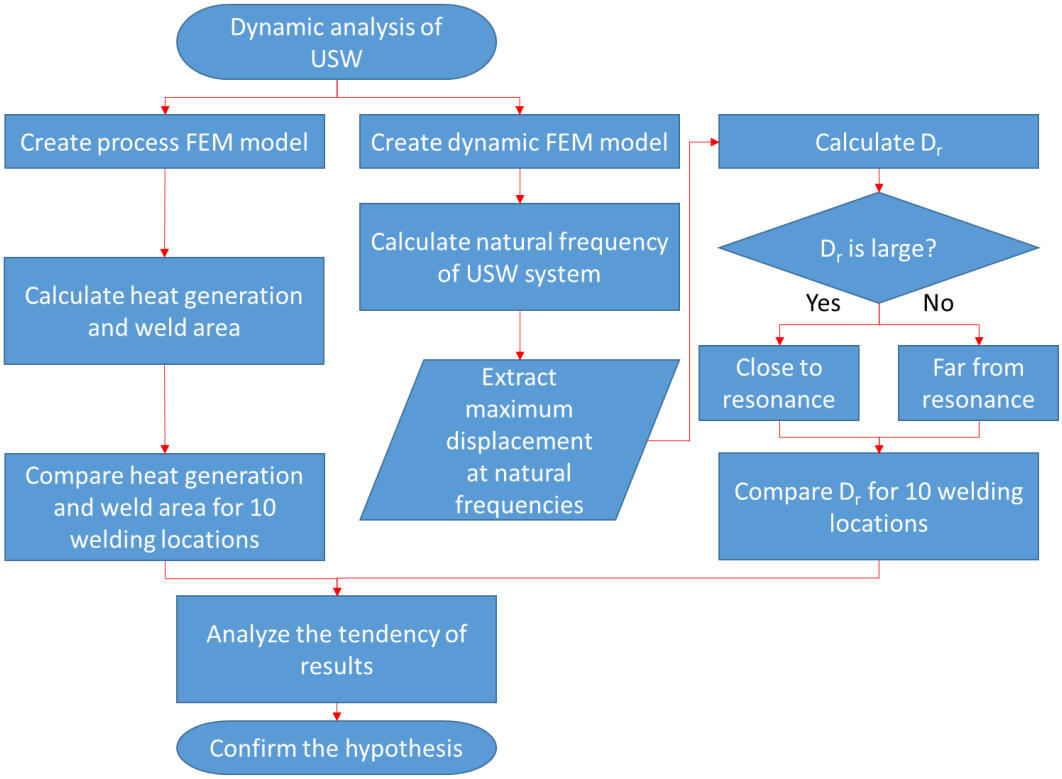

Figure 5.3 Flow chart for the dynamic analysis of USW

Thus, in Section 5.1, a Kevin-Voight damping analytical model is used to calculate the loss of vibration energy through the damping of CFRP parts. In Section 5.2, a dynamic FEM model is proposed to analyze the dynamic response of the CFRP parts under USW frequency in different locations. The dynamic response includes calculations of the natural frequencies and their correlation with the displacement of the CFRP parts. And the process FEM model from the Chapter 4 is used to simulate the welding process to determine the weld area and the heat generation of the corresponding welding locations. Thus, an assessment criterion of the weld quality of each spot

will be proposed by correlating weld area, heat generation and the natural frequency of the parts. Section 5.3 summarizes the chapter with conclusions.

5.1. Analytical Model for Work-Energy Relations in Ultrasonic Welding for CFRP

In this section, an analytical model is built to investigate the dynamic response of the welding system (Figure 5.2). The ultrasonic welding effect will be modeled with a discrete model of a mass-spring-damper system [49, 50].

Figure 5.4(a) is the typical single weld CFRP ultrasonic welding setup while Figure 5.4(b) is a schematic of typical single degree of freedom mass-spring-damper model that represents the fundamental dynamics of ultrasonic welding of CFRP.

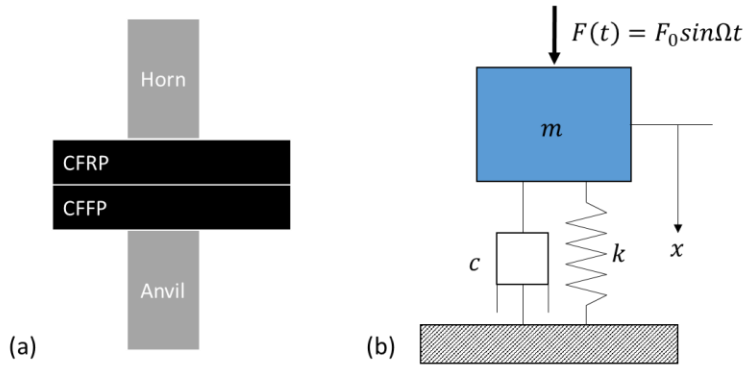

Figure 5.4 Schematics: (a) Typical ultrasonic welding of CFRP, (b) Single degree of freedom mass-spring-damper model (Kevin-Voight damping analytical model)

In Figure 5.4(b), m represents the mass of workpieces under ultrasonic welding which is excited by the horn, k represents the stiffness of the elastic constraint of the workpieces which is the storage modulus of workpieces, and c represent the equivalent viscous damping coefficients of any energy dissipation mechanism which is related with the loss modulus of workpieces.

The welding system is subjected to a harmonic force ($F(t)$) and the displacement is denoted by x. The governing equation of motion for the mass is shown in Equation 5.1.

$$m\ddot{x} + c\dot{x} + kx = F_0 sin\Omega t, \qquad x(0) = \dot{x}(0) = 0 \qquad \text{(Eq. 5.1)}$$

where F_0 is the amplitude of the horn force and Ω (=$2\pi f$, f=vibration frequency in Hz) is the vibration frequency of the horn in rad/s.

From the definition of the mechanical work $dW = F(t)dx = F(t)\dot{x}dt$, the work W performed by the horn oscillation on the workpieces over the first n loading cycles can be expressed as presented in Equation 5.2.

$$W = \int_0^{\frac{2n\pi}{\Omega}} F(t)\dot{x}\, dt = \left(\frac{1}{2}m\dot{x}^2 + \frac{1}{2}kx^2\right)_{t=\frac{2n\pi}{\Omega}} + c\int_0^{\frac{2n\pi}{\Omega}} \dot{x}^2\, dt \qquad \text{(Eq. 5.2)}$$

The first two terms in Equation 5.2 are the kinetic energy (T) and the elastic potential energy (V) at $t = 2n\pi/\Omega$. The third term is the dissipated energy (W_d) by the damping of the system.

Considering the natural frequency $\varpi_n = \sqrt{k/m}$, the damping ratio $\xi = c/2m\varpi_n$ and the static deformation of system $\delta = F_0/k$, Equation 5.1 can be rewritten as Equation 5.3.

$$\ddot{x} + 2\xi\varpi_n\dot{x} + \varpi_n^2 x = \delta\varpi_n^2 sin\Omega t, \qquad x(0) = \dot{x}(0) = 0 \qquad \text{(Eq. 5.3)}$$

The dynamic response of the system $x(t)$ to the harmonic force can be written as Equation 5.4. and divided into the transient solution (first term of Equation 5.4) and the steady state solution (second term in Equation 5.4)

$$x(t) = X_h e^{-\xi\varpi_n t}\sin\left(\sqrt{1-\xi^2}\varpi_d t + \phi_h\right) + Xsin(\Omega t - \phi) \qquad \text{(Eq. 5.4)}$$

where X_h and ϕ_h are the coefficients of the transient response solution which are determined from initial conditions and ϖ_d is the damped natural frequency. X is an amplitude and ϕ is a phase angle of steady state response solution.

Equation 5.5 shows the relations of parameters of Equation 5.4.

$$\varpi_d = \varpi_n\sqrt{1-\xi^2} \qquad X = \frac{\delta}{\sqrt{(1-r^2)^2+(2\xi r)^2}} \quad \phi = \tan^{-1}\left(\frac{2\xi r}{1-r^2}\right) \qquad r = \frac{\Omega}{\varpi_n} \qquad \text{(Eq. 5.5)}$$

For the underdamped system ($\xi < 1$), when the system reaches the settling time ($t_s = 4/\xi\varpi_n$), the system is on the steady state and the transient part of the dynamic response can be negligible [74]. Therefore the dynamic response in Equation 5.4 will be $x(t) = Xsin(\Omega t - \phi)$. It gives the work done per cycle (w) as Equation 5.6 and the dissipated energy per cycle (w_d) as Equation 5.7.

$$w = \int_{\frac{\phi}{\Omega}}^{\frac{(2\pi-\phi)}{\Omega}} F(t)\dot{x}dt = \pi F_0 X sin\phi \qquad \text{(Eq. 5.6)}$$

$$w_d = \int_{\frac{\phi}{\Omega}}^{\frac{(2\pi-\phi)}{\Omega}} c\dot{x}^2 dt = \pi c\Omega X^2 \qquad \text{(Eq. 5.7)}$$

When $\phi = 90°$, corresponding to the resonance, w and w_d will become the same as Equation 5.8 meaning that the whole work done by the oscillation of horn will become the dissipated energy at the resonance.

$$w = w_d = \frac{2\pi\xi r}{(1-r^2)^2+(2\xi r)^2} F_0\delta \qquad \text{(Eq. 5.8)}$$

5.2. Dynamic FEM Model for the Dynamic Response of Ultrasonic Welding for CFRP

In this section, a dynamic FEM model for the joining configuration presented in Figure 5.2 is developed to analyze the dynamic response during ultrasonic welding. This dynamic FEM model is used for calculations of the natural frequency and the displacement of CFRP parts at the natural frequency. The dynamic FEM model is built in Abaqus Standard v14.1, implicit scheme. The material properties of the CFRP parts are the same as used in Chapter 4.

5.2.1. Geometry and Boundary Conditions

The geometry and the boundary conditions are the most important parameters in this model when investigating the vibration characteristics associated with the different welding locations. The model consists of four parts: one U-shaped CFRP part, one flat CFRP part, an upper horn, and an anvil which is fixed (all displacement and rotations are zero). To reproduce the robotic welding conditions, the anvil described in Chapter 4 as a plate is currently modeled as an underneath horn which supports the parts. Figure 5.5 (a) and (b) shows the geometry and the boundary conditions in the FEM model.

For the sake of minimizing the computation time, a symmetry boundary condition set was added to the welding conditions, to simulate one half of the U-channel and the flat surface. Both horns are cylindrical with a diameter of 18 mm and a flat surface. The following degrees of freedom are defined for the four parts:

- *U-shaped and flat parts*: Fixed in the X, Y, Z axis at both side edges
- *Upper horn*: Fixed in the X, Y, Z axis at the both side edges
- *Bottom horn*: Fixed in the X, Y, Z axis at the bottom surface

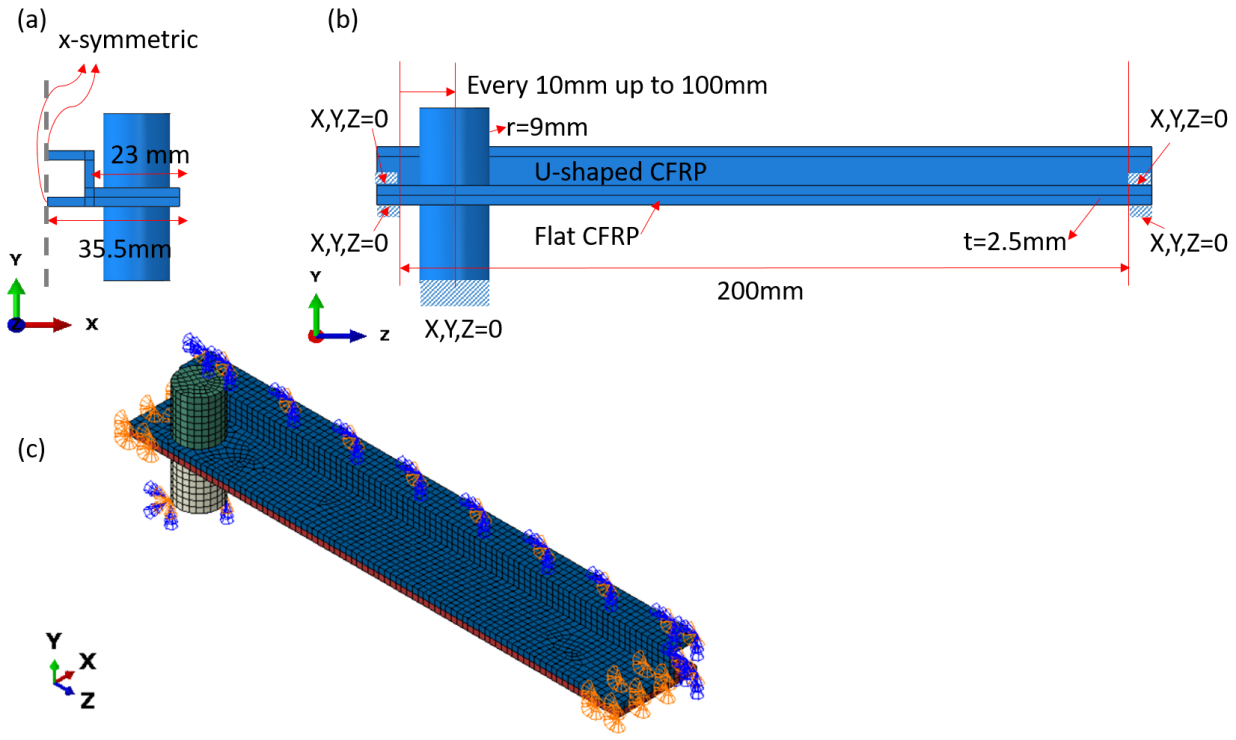

Figure 5.5 Geometry and boundary conditions in the finite element model: (a) Lateral view of the U-shaped and flat parts in contact with the upper and bottom horns, (b) Front view of the parts to be joined where the first spot is set-up for welding and (c) Isometric view of the assembly of the parts with elements

5.2.2. Meshing and Material Properties

The CFRP parts were meshed using a continuous 3-D brick element (C3D8) of 2.5 mm size which is the thickness of CFRP parts. The horn and the anvil were meshed with the same size and type of finite element. As mentioned in the prior section, the same material properties from the ultrasonic welding process FEM model in Chapter 4 are applied in the FEM model for the dynamic response in this section.

5.2.3. Dynamic Response of the Welding System

Natural frequency, also considered as eigenvalues of frequency in dynamic response system, is the frequency at which a system tends to oscillate in the absence of any driving or damping force.

Ultrasonic welding process is an oscillating system driven with a trigger force (mechanical clamping force) at the frequency at which the amplitude of its motion is greatest, e.g. 20 kHz. When this frequency is close to the natural frequency of the oscillating system, this frequency is called resonant frequency. To calculate the natural frequency of the welding system, the Lanczos eigensolver algorithm implemented in Abaqus is applied [73]. The algorithm involves the following steps:

1. Applying the trigger force by clamping the U-shape and flat parts through restricting the displacement in Y-direction (Figure 5.5 (a)) in the weld area of each spot;
2. Extracting of the mass matrix and calculating the natural frequency ω_n.
3. Applying a frequency sweep to the welding system with values nearby the welding frequency (20,000Hz), in a range of [19,920Hz, 20,080Hz] for all ten spots.
4. Plotting the relative displacement of the U-shaped CFRP and the flat CFRP for each frequency and spot (Figure 5.6).

5.2.4. Relative Displacement Index

Using the algorithm presented in Section 5.2.3., the relative displacements of the two parts are extracted for each sweeping frequency and welding spot location and plotted (Figure 5.6). Figure 5.6 shows that there is a large variation of the displacement of CFRP parts according to the natural frequencies with different maximum and minimum values from one welding spot to the other.

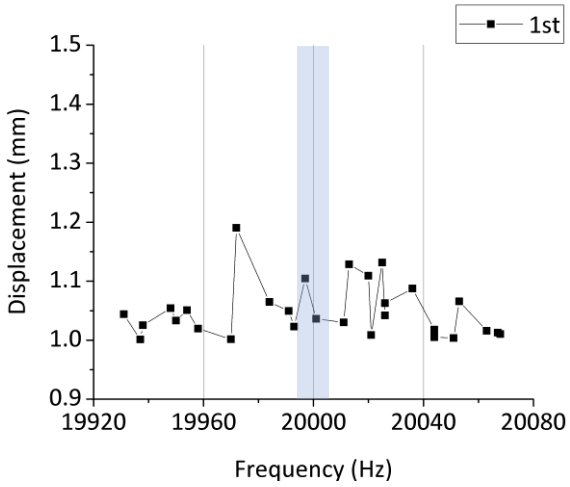
1st
Displacement (mm)
Frequency (Hz)
1.5
1.4
1.3
1.2
1.1
1.0
0.9
19920
19960
20000
20040
20080

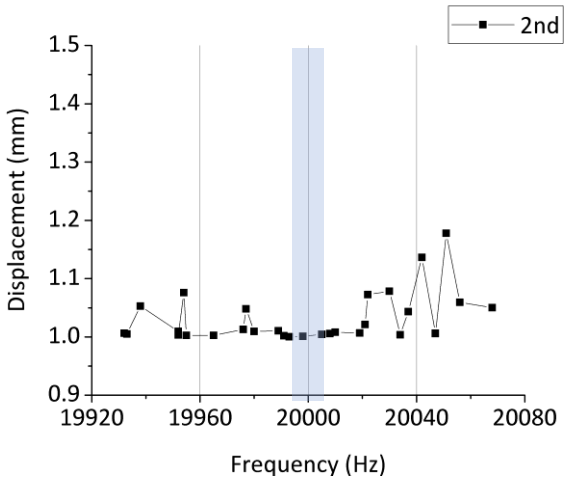
2nd
Displacement (mm)
Frequency (Hz)
1.5
1.4
1.3
1.2
1.1
1.0
0.9
19920
19960
20000
20040
20080

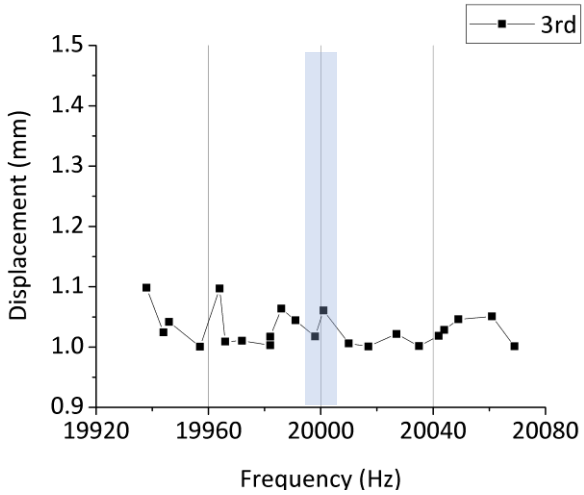
3rd
Displacement (mm)
Frequency (Hz)
1.5
1.4
1.3
1.2
1.1
1.0
0.9
19920
19960
20000
20040
20080

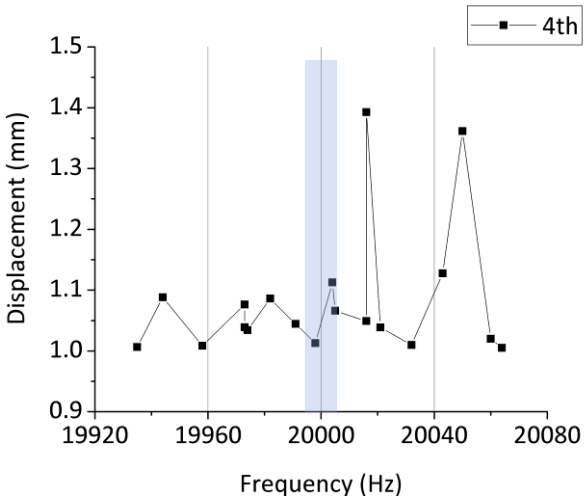
4th
Displacement (mm)
Frequency (Hz)
1.5
1.4
1.3
1.2
1.1
1.0
0.9
19920
19960
20000
20040
20080

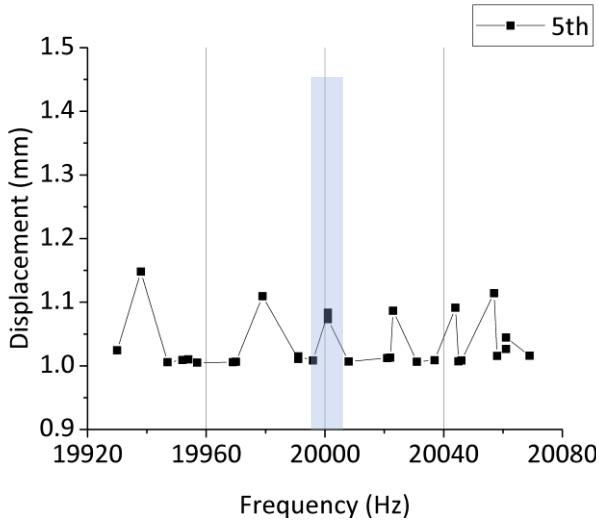
5th
Displacement (mm)
Frequency (Hz)
1.5
1.4
1.3
1.2
1.1
1.0
0.9
19920
19960
20000
20040
20080

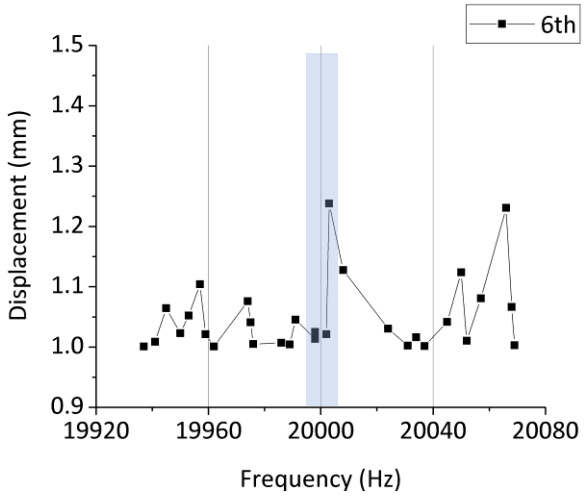
6th
Displacement (mm)
Frequency (Hz)
1.5
1.4
1.3
1.2
1.1
1.0
0.9
19920
19960
20000
20040
20080

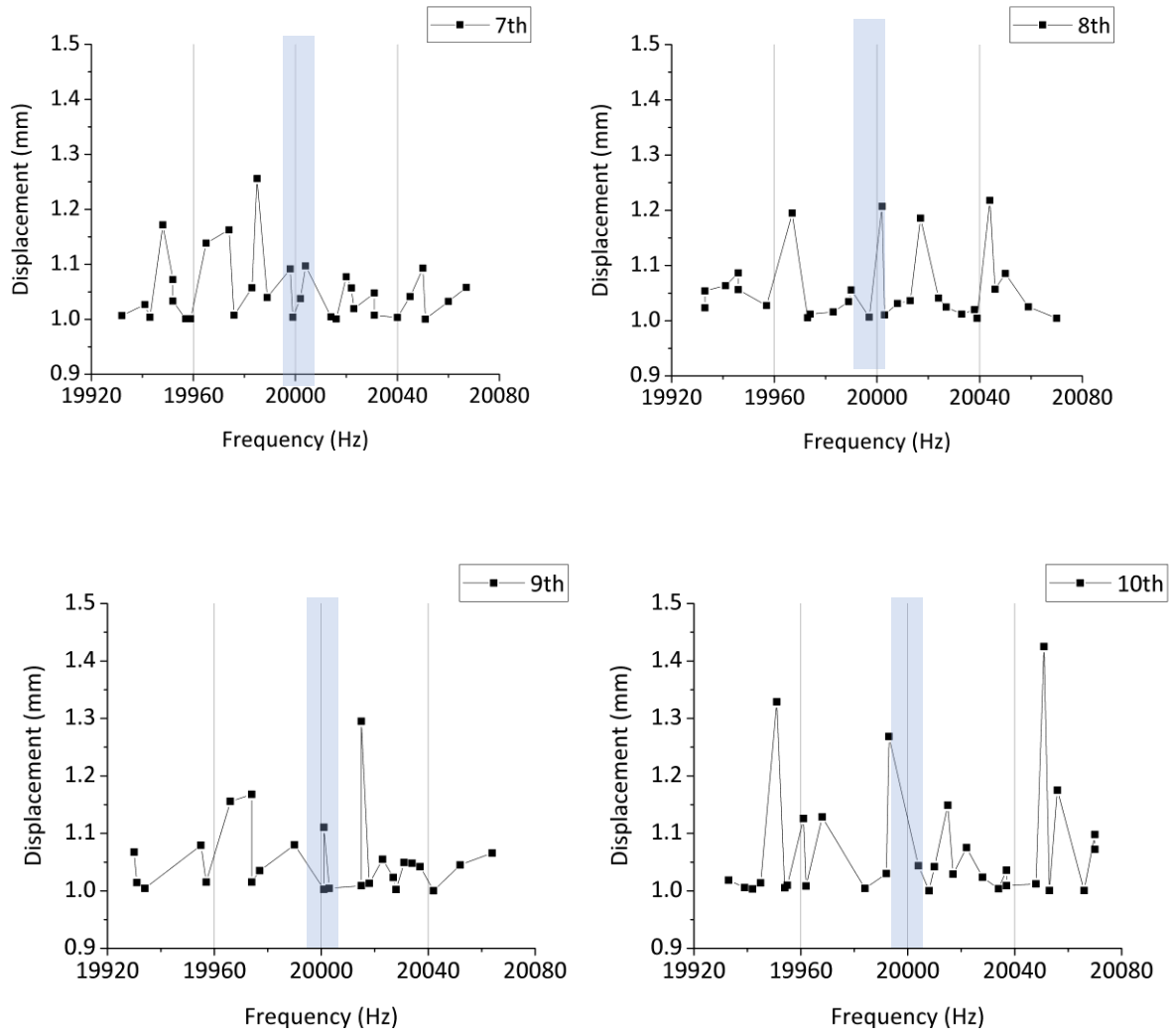

Figure 5.6 Displacements at the natural frequencies in 10 cases according to the welding locations shown in Figure 5.2. A window of ± 4 Hz was used to verify the relative displacement near 20 kHz.

To quantify this diversity of the results and find a solution to sort them, a relative displacement D_r index is introduced. D_r is the ratio between the displacement found at the range of 20 kHz ± 4 Hz and the maximum displacement produced at sweeping frequencies for the same welding spot.

$$D_r = \frac{Displacement\ at\ [20\ \text{kHz}\ \pm\ 4\ \text{Hz}\,]}{Maximum\ displacements\ for\ [19.92\ kHz - 22.08\ kHz]}$$

To understand the role of a low, medium or high value of D_r, the FEM is used for simulation of the welding process for the ten welding spots. For each welding spot, the weld formation heat generation and weld area will be analyzed and correlated with the relative displacement calculated in Section 5.2.4.

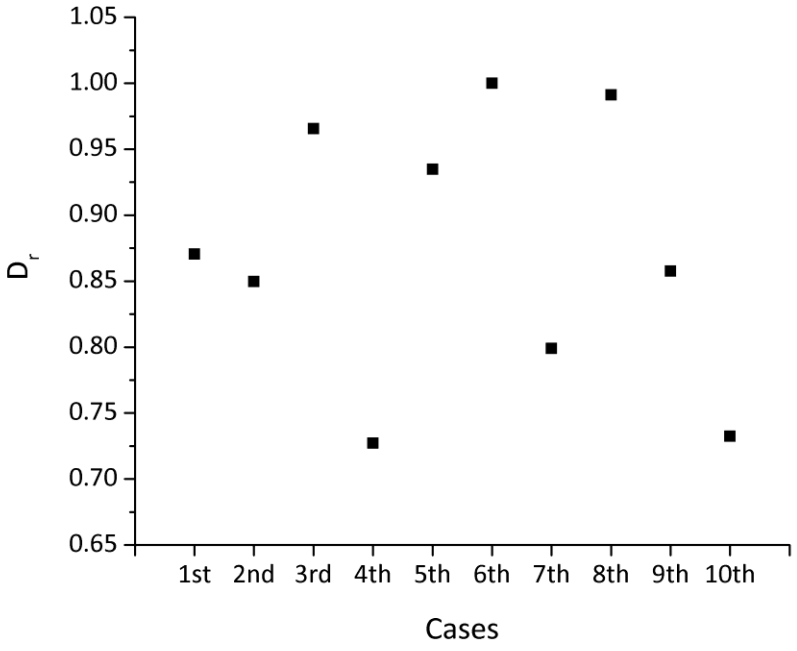

Figure 5.7 Representation of the relative displacement index for all 10 welding spots

5.2.5. Heat Generation and Weld Area Calculation

The process FEM models based on the FEM model developed in Chapter 4 are used to calculate the heat generation and the weld area evolutions with the same boundary conditions of 10 welding locations in Figure 5.2.

Heat generation during ultrasonic welding process can be calculated by the summation of heat generation in each element. The heat generation per element is calculated with Equation 5.9.

$$E_H = \int_{t_0}^{t_1} \rho c(T) \delta T(t) dt dV \qquad \text{(Eq. 5.9)}$$

where ρ is density, c is heat capacity and T is temperature depending on time t in the volume of element V.

The evolution of heat energy generation for 10 cases are shown in Figure 5.8(a). The weld area is calculated by summation of elements' surface area which have higher temperature than the melting temperature. The evolution of weld area for 10 cases are shown in Figure 5.9(a). There is a general correlation of weld area and heat generation for all 10 cases as is expected. To determine the correlation, the values of the heat generation and the weld area at 0.3 second are compared because the dynamic response is related to the beginning of the welding process (Figure 5.8(b) and Figure 5.9(b)).

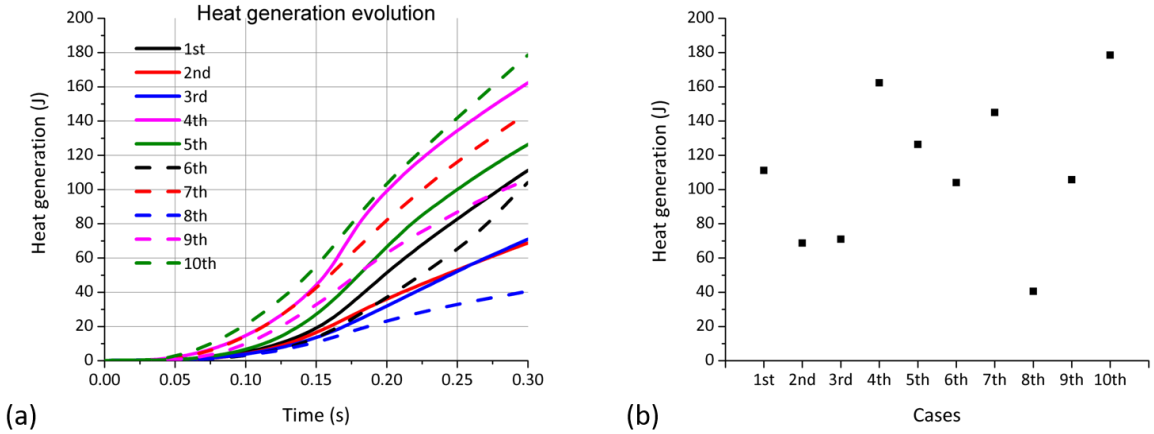

Figure 5.8 Heat generation evolution during ultrasonic welding for the 10 cases: (a) Heat generation evolution with welding time, (b) Heat generation corresponding to each case at 0.3s welding time.

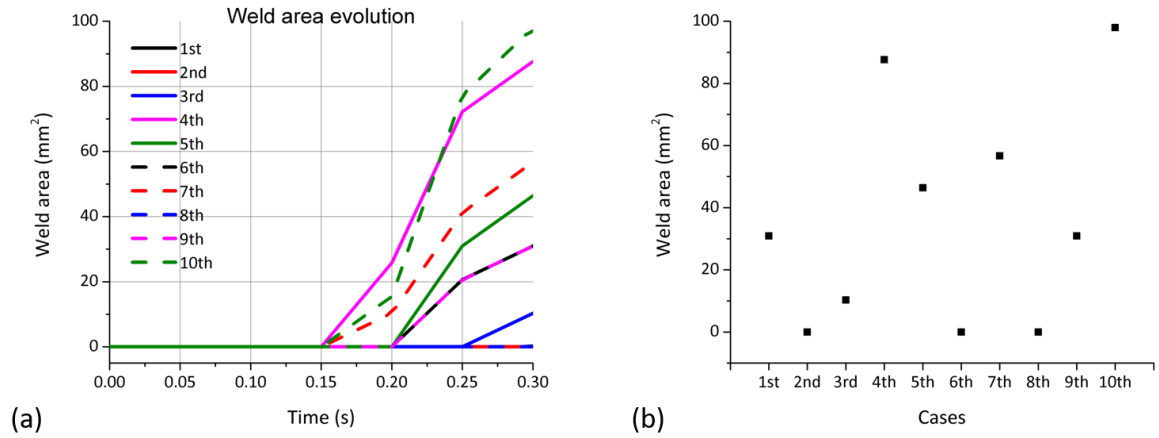

Figure 5.9 Weld area evolution during ultrasonic welding for 10 cases: (a) Weld area evolution with welding time, (b) Weld area corresponding to each case at 0.3s welding time

Figures 5.8 and Figure 5.9 indicate that cases 4^{th}, 7^{th} and 10^{th} have the highest energy due to the highest heat generation and the largest weld area. In figure 5.7, it is noticed that D_r has the lowest value for these cases. These attributes of the weld correspond to *a good quality weld*. The 1^{st}, 5^{th} and 9^{th} cases have a lower heat generation and weld area which correspond to a *moderate quality weld*. For the same cases, D_r has an average value. The 2^{nd}, 3^{rd}, 6^{th} and 8^{th} cases have the lowest heat generation and weld area corresponding to a *poor quality weld*. D_r has the highest values for these cases except 2^{nd} case.

It can be noticed that D_r is inversely proportional to the heat generation and weld quality. In other words, a large relative displacement of the two parts is preferable to resonant motion of welding system, which leads to dissipation of the energy and consequently an inefficient weld formation. Figure 5.10 shows the comparison of the generation, the weld area and the inverse of the relative displacement index $(1/D_r)$ which confirms the trends of the changes of the three values correspond.

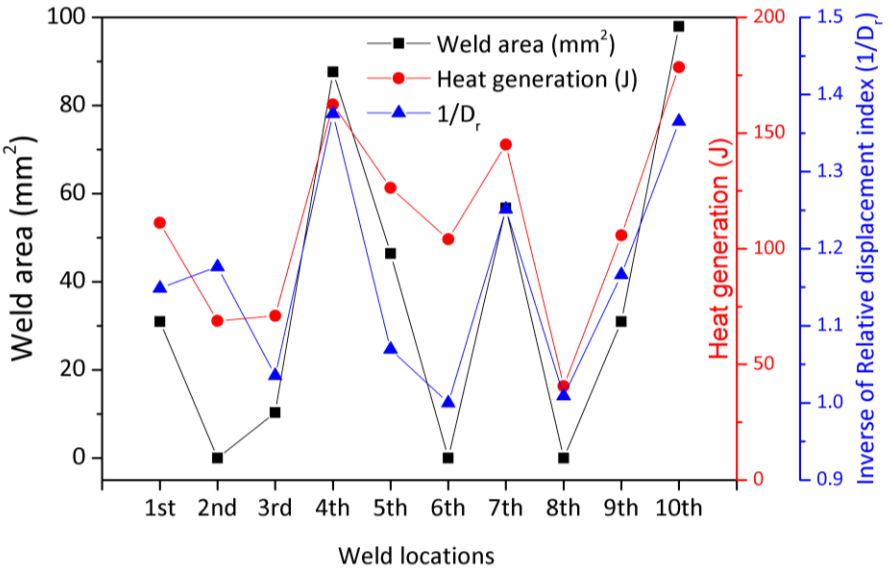

Figure 5.10 Weld area, heat generation and the inverse of the relative displacement index $(1/D_r)$

5.3. Conclusion

In this chapter, an analytical and a FEM model were developed and used for dynamic analysis of a multi-spot welding system using USW. Thus, the displacement of the two CFRP parts were analyzed for each welding spot. A relative displacement index was proposed to characterize the weld quality. For assessing the weld quality using the relative displacement index, a correlation between this index and simulated heat generation and weld area was done. Base on this assessment, it can be concluded that:

(1) Ultrasonic welding of CFRP can be affected by the boundary conditions due to their different vibration characteristics.

(2) Significant vibrational energy loss can occur when the natural frequency is close to the oscillation frequency in ultrasonic welding of CFRP.

(3) These results can be used to guide the design process for multi-spot welding of complex parts.

Chapter 6 Summary and Future Work

6.1. Summary

Ultrasonic welding of CFRP without energy directors is investigated both experimentally and numerically to obtain a fundamental understanding of the heating phenomenon during welding. Novel research has been conducted on the modeling of ultrasonic welding process via finite element method which provides a new approach for achieving a more robust welding quality.

Morphological parameters are introduced and controlled via an annealing process for ultrasonic welding. The degree of crystallinity and α/γ ratio are measured experimentally before and after annealing with various annealing temperatures. The results show that the weld performance is influenced by the increase of annealing temperature which leads to a stable degree of crystallinity and increase of α/γ ratio.

Temperature dependent mechanical properties are defined and measured to construct a finite element model of ultrasonic welding process for CFRP without energy directors. From the results of the FEM model, the heat generation mechanisms are shown for the ultrasonic welding process. The effect of the morphological parameters in ultrasonic welding process of CFRP was investigated and confirmed that the results of FEM model corresponded with experimental results. To validate the model, the temperature profile and weld area evolution are measured and compared with simulation results.

To understand the variation of welding performance with small different boundary conditions, the investigation of the dynamic response of ultrasonic welding process of CFRP was conducted using another FEM model. This FEM model confirmed that the displacement at the natural

frequency of the CFRP workpieces other than the welding locations becomes larger which leads to the resonance and high dissipated energy from the vibration energy. These phenomena result in poor welding performance.

The major findings of this dissertation can be summarized in three parts:

(1) Influence of morphological parameters on welding process and weld performance of CFRP by ultrasonic welding:

- Morphological parameters, such as the DoC and the α/γ ratio, influence the material viscoelastic and mechanical properties, which are important parameters for USW. Morphological parameters must be considered to control the USW performance.
- Annealing can be used to control the material's morphological parameters, inducing a uniform DoC distribution. The α/γ ratio increases with annealing temperature.
- The uniform DoC and increased α/γ ratio obtained by annealing increase the storage and loss moduli and the glass transition temperature of the material, which results in more efficient USW, in terms of heat generation by interfacial and intermolecular friction. These changes in the morphological parameters also cause the material to have a higher ultimate tensile strength.
- The improved viscoelastic and mechanical properties lead to higher average and less variable weld strengths.

(2) Process modeling of ultrasonic welding of carbon fiber reinforced plastics without energy directors:

- The interfacial friction heating is dominant at the beginning of the USW process (about 0.2-0.4s).

- The intermolecular friction heating becomes dominant after the glass transition temperature is reached in the matrix (after 0.4s).
- The heat generation rate produced by interfacial friction heating are dominant in the proximity of the edges of the horn and the heat generation rate produced by intermolecular friction heating is dominant under the center of horn.
- The heat generation rate is higher closer to the edges of the horn because of two heating mechanisms which results in the beginning of melting at the area under the edge of the horn.
- The weld forms at the edge in the beginning and propagates toward to the center which might lead to the unstable weld strengths for the poor welding without energy directors.

(3) Dynamic analysis of ultrasonic welding of CFRP according to boundary conditions:

- Ultrasonic welding of CFRP can be affected by the boundary conditions due to their different vibration characteristics.
- From the displacement analysis at the natural frequencies, it is confirmed that significant vibrational energy loss can occur when the natural frequency is close to the oscillation frequency in ultrasonic welding of CFRP
- These results can be used to guide the design process of the multi-spot welding of complex parts.

6.2. Future Work

Based on the findings on the dissertation, several topics for future research are suggested as below:

(1) Multi spot ultrasonic welding process analysis for the welding performance prediction

Joints in assembly by ultrasonic welding consist of multi spot welds to provide enough joint strength and cover entire overlapped areas of an assembly. There have been many researches on the single spot ultrasonic welding. However, the study of multi-spot ultrasonic welding has not been conducted despite the need for industry to apply the multi-spot ultrasonic welding for their applications. This study will provide sufficient and practical knowledge for using the ultrasonic welding in the assembly process.

(2) Hybrid joining technologies with different joining technologies (i.e. adhesive bonding)

Hybrid joining technology is one of the promising candidates for multi-materials joining. Ultrasonic welding (USW), is one joining technology with fast processing speed based on spot joint design. USW provides mechanical interlocking between two substrates which is not available in adhesive bonding. By combining two different joining technologies, the mechanical performance will be improved and the manufacturing cost will be reduced by replacing the fixture to hold the substrates for curing.

Bibliography

[1] Das, T. K., Ghosh, P., and Das N., 2019, "Preparation, development, outcomes, and application versatility of carbon fiber-based polymer composites: a review," Advanced Composites and Hybrid Materials, pp.1-20

[2] Yao, S. S., Jin, F.-L., Rhee, K. Y., Hui, D., and Park, S.-J, 2018, "Recent advances in carbon- fiber-reinforced thermoplastic composites: A review," Composites: Part B, 142, pp.241-250

[3] Lyu, M.-Y. and Choi, T. G., 2015, "Research Trends in Polymer Materials for Use in Lightweight Vehicles," International Journal of Precision Engineering and Manufacturing, 16(1), pp.213-220

[4] Yancey, R. N., 2016, "2- Challenges, opportunities, and perspectives on lightweight composite structures: aerospace versus automotive," Lightweight Composite Structures in Transport: Design, Manufacturing, Analysis and Performance, pp. 35-52.

[5] Ageorges, C., Ye, L. and Hou, M., 2001, "Advances in fusion bonding techniques for joining thermoplastic matrix composites: a review", Composites: Part A, 32, pp.839-857.

[6] Grewell, D. and Benatar A., 2007, "Welding of Plastics: Fundamentals and New Developments," International Polymer Processing, 22, pp.43-60

[7] Jeevi, G., Nayak S. K. and Kader M. A., 2019, "Review on adhesive joints and their application in hybrid composite structures," Journal of Adhesion Science and Technology, 33(14), pp. 1497-1520

[8] Rashli, R., Bakar, E. A., Kamaruddin, S. and Othman, A. R., 2013, "A Review of Ultrasonic Welding of Thermoplastic Composites," Caspian Journal of Applied Sciences Research, 2(3), pp. 01-16

[9] Benatar, A. and Gutowski, T. G., 1989, "Ultrasonic Welding of PEEK Graphite APC-2 Composites," Polymer Engineering and Science, 29(23), pp.1705-1721

[10] Wang, K., Shriver, D., Li, Y., Banu, M., Hu, S. J., Xiao, G., Arinez, J and Fan, H.-T., 2017, "Characterization of weld attributes in ultrasonic welding of short carbon fiber reinforced thermoplastic composites," Journal of Manufacturing Processes, 29, pp. 124-132

[11] Wang, K., Shriver, D., Banu, M., Hu, S. J., Xiao, G., Arinez, J. and Fan, H.-T., 2017 "Performance Prediction for, Ultrasonic Spot Welds of Short Carbon Fiber-Reinforced Composites Under Shear Loading," Journal of Manufacturing Science and Engineering, 139(11), pp. 111001

[12] Nash, N.H., Young, T.M., McGrail, P.T. and Stanley, W.F., 2015, "Inclusion of a thermoplastic phase to improve impact and post-impact performances of carbon fibre reinforced thermosetting composites — A review," Materials and Design, 85, pp.582-597

[13] Deng, S., Djukic, L., Paton, R. and Ye, L., 2015, "Thermoplastic–epoxy interactions and their potential applications in joining composite structures – A review," Composites: Part A, 68, pp. 121-132

[14] Wan, Y. and Takahashi, J., 2016, "Tensile and compressive properties of chopped carbon fiber tapes reinforced thermoplastics with different fiber lengths and molding pressures," Composites: Part A, 87, pp. 271-281

[15] Mahajan, G. V. and Aher, V. S., 2012, "Composite Material: A Review over Current Development and Automotive Application," International Journal of Scientific and Research Publications, 2(11), pp.1-5

[16] Mallick, P. K., 2010, "Thermoplastics and thermoplastic–matrix composites for lightweight automotive structures," Chapter 5, Materials, Design and Manufacturing for Lightweight Vehicles, CRC Press, Boca Raton, FL, pp.174-207

[17] Barbero, E. J., 2018, "Introduction to Composite Materials Design," 3rd ed., CRC Press, Boca Raton, FL

[18] Maffezzoli, A., Gennaro, R. and Greco, A., 2012, "Thermoplastic Composite Manufacturing Cost Analysis," Wiley Encyclopedia of Composites, 2nd ed., John Wiley & Sons, Inc.

[19] Barile, C., Casavola, C. and Cillis, F. D., 2019, "Mechanical comparison of new composite materials for aerospace applications," Composites: Part B, 162, pp. 122-128

[20] Gabr., M. H., Okumura, W., Ueda, H., Kuriyama, W., Uzawa, K. and Kimpara, I., 2015, "Mechanical and thermal properties of carbon fiber/polypropylene composite filled with nano-clay," Composites: Part B, 69, pp.94-100

[21] Pal K., Panwar, V., Friedrich, S. and Gehde, M., 2016, "An Investigation on Vibration Welding of Amorphous and Semicrystalline Polymers," Materials and Manufacturing Processes, 31, pp. 372-378

[22] Leon, A. C. D., Chen, Q., Palaganas, N. B., Palaganas, J. O., Manapat, J. and Advincula, R. C., 2016, "High performance polymer nanocomposites for additive manufacturing applications," Reactive and Functional Polymers, 103, pp. 141-155

[23] Vaidya, U. K. and Chawla, K. K., 2008, "Processing of fibre reinforced thermoplastic composites," International Materials Reviews, 53(4), pp. 185-218

[24] Kelly G., 2004, "Joining of Carbon Fibre Reinforced Plastics for Automotive Applications," PhD Thesis, Royal Institute of Technology, Sweden

[25] Costa1, A. P., Botelho, E. C., Costa, M. L., Narita, N. E. and Tarpani, J. R., 2012, "A Review of Welding Technologies for Thermoplastic Composites in Aerospace Applications," Journal of Aerospace Technology and Management, 4(3), pp. 255-265

[26] Yousefpour, A., Hohhati, M. and Immarigeon, J.-P., 2004, "Fusion Bonding/Welding of Thermoplastic Composites," Journal of Thermoplastic Composite Materials, 17, pp. 303-341

[27] Wagner, G., Balle, F. and Eifler, D., 2013, "Ultrasonic Welding of Aluminum Alloys to Fiber Reinforced Polymers," Advanced Engineering Materials, 15(9), pp. 792-803

[28] Ting, E. C. and Tuan, J. L., 1973, "Dissipative Heating in a Viscoelastic Material Due to Cyclic Pressure," Transactions of the society of rheology, 17(2), pp. 209-225

[29] Tolunay, M. N., Dawson, P. R. and Wang, K. K., 1983, "Heating and Bonding Mechanisms in Ultrasonic Welding of Thermoplastics," Polymer Engineering and Science, 23(13), pp.726-733

[30] Zhang, Z., Wang, X., Luo, Y., Zhang, Z. and Wang, L., 2010, "Study on Heating Process of Ultrasonic Welding for Thermoplastics," Journal of Thermoplastic Composite Materials, 23, pp. 647-664

[31] Villegas, I. F., 2015, "In situ monitoring of ultrasonic welding of thermoplastic composites through power and displacement data," Journal of Thermoplastic Composite Materials, 28(1), pp. 66-85

[32] Harras, B., Cole, K. C. and Vu-Khanh, T., 1996, "Optimization of the Ultrasonic Welding of PEEK-Carbon Composites," Journal of Reinforced Plastics and Composites, 15, pp. 174-182

[33] Liu, S.-J. and Chang, I-T., 2001, "Factors Affecting the Joint Strength of Ultrasonically Welded Polypropylene Composites," Polymer Composites, 22(1), pp.132-141

[34] Liu, S.-J. Lin, W.-F., Chang, B.-C. and Wu, G.-M, 1999, "Optimizing the Joint Strengthof Ultrasonically Welded Thermoplastics," Advances in Polymer Technology, 18(2), pp. 125-135

[35] Liu, S.-J. and Chang, I-T., 2002, "Optimizing the Weld Strength of Ultrasonically Welded Nylon Composites," Journal of Composite Materials, 36(5), pp. 611-624

[36] Villegas, I. F. and Bersee, H. E. N., 2010, "Ultrasonic Welding of Advanced Thermoplastic Composites: An Investigation on Energy-Directing Surfaces," Advances in Polymer Technology, 29(2), pp. 112-121

[37] Villegas, I. F., Grande B. V., Bersee, H. E. N. and Benedictus, R., 2015, "A comparative evaluation between flat and traditional energy directors for ultrasonic welding of CF/PPS thermoplastic composites," Composite Interfaces, 22(8), pp. 717-729

[38] Palardy, G. and Villegas, I. F., 2017, "On the effect of flat energy directors thickness on heat generation during ultrasonic welding of thermoplastic composites," Composite Interfaces, 24(2), pp. 203-214

[39] Chuah, Y. K., Chien L.-H., Chang, B. C. and Liu, S.-J., 2000, "Effects of the Shape of the Energy Director on Far-Field Ultrasonic Welding of Thermoplastics," Polymer Engineering and Science, 40(1), pp.157-167

[40] Zhi, Q., Tan, X. R. and Liu, Z. X., 2017, "Effect of Moisture on the Ultrasonic Welding of Carbon Fiber Reinforced Polyamide 66 Composite," Welding Journal, 96, pp. 185-192

[41] Wang, K., Li, Y., Banu, M., Li, J., Guo, W. and Khan, H., 2017, "Effect of interfacial preheating on welded joints during ultrasonic composite welding," Journal of Materials Processing Technology, 246, pp. 116-122

[42] Wang, X., Yan, J., Li, R. and Yang, S., 2006, "FEM Investigation of the Temperature Field of Energy Director during Ultrasonic Welding of PEEK Composites," Journal of Thermoplastic Composite Materials, 19, pp. 593-607

[43] Suresh, K. S., Rani, M. R., Prakasan, K., and Rudramoorthy, R., 2007, "Modeling of temperature distribution in ultrasonic welding of thermoplastics for various joint designs," Journal of Materials Processing Technology, 186, pp. 138-146

[44] Levy, A., Corre S. L. and Poitou, A., 2014, "Ultrasonic welding of thermoplastic composites: a numerical analysis at the mesoscopic scale relating processing parameters, flow of polymer and quality of adhesion," International Journal of Material Forming, 7, pp. 39-51

[45] Levy, A., Corre S. L. and Villegas, I. F., 2014, "Modeling of the heating phenomena in ultrasonic welding of thermoplastic composites with flat energy directors," Journal of Materials Processing Technology, 214, pp. 1361-1371

[46] Levy, A., Corre S. L., Poitou, A. and Soccard E., 2011, "Ultrasonic Welding of Thermoplastic Composites: Modeling of the Process Using Time Homogenization," Journal for Multiscale Computational Engineering, 9(1), pp. 53-72

[47] Kang, B., Cai, W. W., and Tan, C.-A,, 2013, "Dynamic Response of Battery Tabs Under Ultrasonic Welding," Journal of Manufacturing Science and Engineering, 135(5), pp. 051013

[48] Kang, B., Cai, W. W., and Tan, C.-A,, 2014, "Dynamic Stress Analysis of Battery Tabs Under Ultrasonic Welding," Journal of Manufacturing Science and Engineering, 136(4), pp. 041011

[49] Kang, B., Cai, W. W., and Tan, C.-A,, 2014, "Vibrational energy loss analysis in battery tab ultrasonic welding," Journal of Manufacturing Processes 16, pp. 218–232

[50] Lee, S. S., Kim, T. H., Cai, W. W., and Abell, J. A., 2014, "Parasitic vibration attenuation in ultrasonic welding of battery tabs," The International Journal of Advanced Manufacturing Technology, 71, pp. 181–195

[51] Luo, Y., Zhang, Z., Wang, X. and Zheng, Y., 2010, "Ultrasonic bonding for thermoplastic microfluidic devices without energy director," Microelectronic Engineering, 87, pp. 2429-2436

[52] Li, Y., Arinez, J., Liu, Z., Lee, T. H., Fan, H.-T., Xiao, G.,Banu, M., and Hu, S. J., 2018, "Ultrasonic welding of carbon fiber reinforced composite with variable blank holding force," ASME Journal of Manufacturing Science and Engineering, 140(9), pp. 091011

[53] Crompton, T. R., 1993, "Degree of Crystallinity and Melting Temperature," Practical Polymer Analysis, Springer, Boston, MA.

[54] Cartledge, H.C.Y. and Baillie, C.A., 1999, "Studies of microstructural and mechanical properties of nylon/glass composite Part I The effect of thermal processing on crystallinity, transcrystallinity and crystal phases," Journal of Material Science, 34(20), pp. 5099-5111

[55] Fornes, T. D. and Paul, D. R., 2003, "Crystallization behavior of nylon 6 nanocomposites," Polymer, 44(14), pp. 3945-3961

[56] Dasgupta, S., Hammond, W. B. and Goddard, W. A., 1996, "Crystal structures and properties of nylon polymers from theory," Journal of American Chemical Society, 118(49), pp. 12291-12301

[57] Karsli, N. G. and Aytac, A., 2013, "Tensile and thermomechanical properties of short carbon fiber reinforced polyamide 6 composites," Composites: Part B, 51, pp. 270-275

[58] Liang, J., Xu, Y., Wei, Z., Song, P., Chen, G. and Zhang, W., 2014, "Mechanical properties, crystallization and melting behaviors of carbon fiber-reinforced PA6 composites," Journal of Thermal Analysis and Calorimetry, 115(1), pp. 209-218

[59] Hu, X. and Zhao, X., 2004, "Effects of annealing (solid and melt) on the time evolution of polymorphic structure of PA6/silicate nanocomposites," Polymer, 45(11), pp. 3819-3825

[60] Xie, S., Zhang, S., Liu, H., Chen, G., Feng, M., Qin, H., Wang, F. and Yang, M., 2005, "Effects of processing history and annealing on polymorphic structure of nylon-6/montmorillonite nanocomposites," Polymer, 46(14), pp. 5417-5427

[61] Yan, X., Imai, Y., Shimamoto, D. and Hotta, Y., 2014, "Relationship study between crystal structure and thermal/mechanical properties of polyamide 6 reinforced and unreinforced by carbon fiber from macro and local view," Polymer, 55(23), pp. 6186-6194.

[62] Nonhof, C. J. and Luiten, G. A., 1989, "Estimates for process conditions during the ultrasonic welding of thermoplastics," Polymer Engineering and Science, 36(9), pp. 1177-1183

[63] Levy, A., Corre S. L. Chevaugeon, N. and Poitou A., 2011, "A level set based approach for the finite element simulation of a forming process involving multiphysics coupling: Ultrasonic welding of thermoplastic composites," European Journal of Mechanics A/Solids, 30, pp. 501-509

[64] Chung, Y. M., 2006, "Microstructure of vibration welded joints of polyamide-6," PhD Thesis, McGill University, Montreal, Canada.

[65] Russell, D. P. and Beaumont, P. W. R., 1980, "Structure and properties of injection-moulded nylon-6," Journal of Material Science, 15(1), pp. 197-207

[66] Wang, C. and Ying, S., 2013, "Thermal, Tensile and Dynamic Mechanical Properties of Short Carbon Fibre Reinforced Polypropylene Composites," Polymers and Polymer Composites, 21(2), pp. 65-72

[67] Menard, K. P. and Menard, N. R., 2015, "Dynamic Mechanical Analysis in the Analysis of Polymers and Rubbers," Encyclopedia Polymer Science and Technology, pp. 1–33

[68] Tutunjian, S., Eroglu, O., Dannemann, M., Modler, N. and Fischer, F., 2019, "A numerical analysis of an energy directing method through friction heating during the ultrasonic welding of thermoplastic composites," Journal of Thermoplastic Composite Materials, pp. 1–19

[69] Fu, S.-Y. and Mai, Y.-W., 2003, "Thermal conductivity of misaligned short-fiber-reinforced polymer composites," Applied Polymer, 88(6), pp. 1497-1505.

[70] Joven, R., 2012, "Thermal properties of carbon fiber/epoxy composites with different fabric weaves," SAMPE International Symposium Proceedings

[71] Pradère C., Goyhénèche, J. M., Batsale, J. C., Dilhaire, S. and Pailler, R., 2005, "Specific-heat measurement of single metallic, carbon, and ceramic fibers at very high temperature," Review of Scientific Instruments, 76, pp. 064901

[72] Millot, C., Fillot, L.-A., Lame, O., Sotta, P. and Seguela, R., 2015, "Assessment of polyamide-6 crystallinity by DSC: Temperature dependence of the melting enthalpy," Journal of Thermal Analysis and Calorimetry, 122(1), pp. 307-314

[73] Abaqus 6.14 Analysis User's Guides, Simulia

[74] Kang, B., Cai, W. W., and Tan, C.-A,, 2017, "Fundamental Dynamics of ultrasonic welding," Ultrasonic Welding of Lithium-Ion Batteries, Ch.10., Cai, W. W., ASME Press.

[75] Tutunjian, S., Dannemann, M., Modler, N., Kucher, M., and Fellermayer, A., 2020, "A Numerical Analysis of the Temporal and Spatial Temperature Development during the Ultrasonic Spot Welding of Fibre-Reinforced Thermoplastics," Journal of Manufacturing and Materials Processing, 4(30), pp. 1-17